FLORIDA STATE UNIVERSITY
COLLEGE OF ARTS AND SCIENCES

UNDERSTANDING THE EVOLUTION OF TROPICAL CYCLONES THROUGH THE $\psi - \chi$ FRAMEWORK

By

SWETA DAS

A Dissertationsubmitted to the
Department of Earth, Ocean and Atmospheric Science
in partial fulfillment of the
requirements for the degree of
Doctor of Philosophy

[2020]

Sweta Das defended this dissertation on December 5, 2019].

The members of the supervisory committee were:

Dr. Vasubandhu Misra
Professor Directing Dissertation

Dr. Eric Chicken
University Representative

Dr. Guosheng Liu
Co-advisor

Dr. Mark Bourassa
Committee Member

Dr. Jeffrey Chagnon
Committee Member

The Graduate School has verified and approved the above-named committee members, and certifies that the dissertation has been approved in accordance with university requirements.

TABLE OF CONTENTS

LIST OF TABLES

LIST OF FIGURES

ABSTRACT

The understanding of the evolution of a Tropical Cyclone (TC) has been a topic of research for several years. During the hurricane season not all thunderstorm events embedded in the African easterly waves or otherwise evolve into organized convection with a closed low pressure system, manifesting into TCs. In this work we suggest that one of the ways to objectively analyze the evolution of the TC is to understand the evolution of the conversion of the available potential energy into kinetic energy on the scale of the disturbance. This study explores the energetics of the interaction between Streamfunction (Psi: ψ)-Velocity Potential (Chi: χ) in the numerical simulations of the TCs.

Using the output of separate 48-hour WRF simulations of three Atlantic TCs: Cindy and Irma of 2017, and Michael 2018, we analyze the time history of the conversion of their kinetic energy from the irrotational to the non-divergent components of the winds. All of these TCs had varied intensities with Cindy being the weakest and Irma being the strongest over the simulation period, which WRF simulated with reasonable fidelity in the evolution of their peak intensities. We show that at 850hPa, the fractional conversion of the kinetic energy from the irrotational to the non-divergent component of the wind increases as the TC intensifies and is higher for the stronger TCs than weaker TCs. Contrastingly, in the outflow level of the TC this transfer of kinetic energy is weaker for stronger TCs than the weaker TCs. Our analysis reveals that when the gradients of the streamfunction and velocity potential are large and oriented parallel to each other both in the large-scale TC environment and in the region of the primary circulation of the TC, then the TC is favored to intensify with robust conversion of the kinetic energy of the irrotational flow(K_χ) to kinetic energy of non-divergent flow (K_ψ) at 850hPa. In contrast, however in the

outflow layer, we require a slower conversion of K_χ to K_ψ for a TC to intensify otherwise it leads to increased inertial instability and weakening of the TC. We arrive at similar conclusions when we contrast the evolution of the tropical cyclones from its genesis to intensifying stages. Likewise, when we examine the sensitivity of the simulations of the tropical cyclones to the choice of microphysics, we find that parameterizations that engenders strong conversion of K_χ to K_ψ at 850 hPa and weak conversion of K_χ to $K_\psi$at the outflow level leads to the simulation of stronger TCs. Therefore, analyzing this conversion rate of kinetic energy of the flow field helps in understanding the evolution of the intensity of TCs.

CHAPTER 1

INTRODUCTION

In explaining the evolution of the Indian summer monsoon, Krishnamurti and Ramanathan (1982) used the so called psi-chi (or streamfunction-velocity potential) framework that illustrated the time evolution of the transformation of the kinetic energy from irrotational to the non-divergent component of the wind. They showed the progression of the transformation of the Available Potential Energy (APE) to eventually the kinetic energy of the non-divergent component of the wind, which was consistent with the evolution of the kinematic field from onset to maturity and then demise of the Indian summer monsoon. They even used this framework to understand the intraseasonal variations of the Indian summer monsoon. In this study we use the same psi-chi framework to understand the differences in the simulation of three different Atlantic Tropical Cyclones (TCs) that vary in their intensity over the period of their model simulation. The intent here of course is to show the time evolution of the transformation of the energy from the irrotational to the non-divergent component of the wind as the TC evolve and its relation to the lifecycle of the TC in order to propose this as a viable framework to understand the evolution of TC. However, we will also elaborate on the transformation of this energy in the outflow level of the TC, where it takes a different meaning than at the lower levels of the TC.

The interest to understand the evolution of the TC cannot be understated. There are innumerable observational, modeling, and theoretical studies that have been conducted over several decades to understand their evolution and structure (e.g., Shapiro and Willoughby 1982; Emanuel 1986; Black et al. 2007; Elsberry and Harr 2008; Braun et al. 2013; Doyle et al. 2017). Furthermore, there is a growing interest in understanding the role of the TC outflow level in the

modulation of the intensity of the TC (Merill 1988; Rappin et al. 2011; Barrett et al. 2016; Komaromi and Doyle 2017). Our study here will leverage many of the findings of these earlier studies to provide a complimentary viewpoint on the evolution of the TCs.

Krishnamurti and Ramanathan (1982) explored Psi-Chi interactions and set out to provide some understanding of the link between the differential heating and the evolution of the monsoons. The most important findings of this paper in regard to the observed evolution of the Indian summer monsoon were a) the dramatic increase in the kinetic energy of the total flow field and especially of the non-divergent component of the flow field in the lower troposphere over the Indian monsoon domain, b) differential heating (expressed as a latitudinal gradient of diabatic heating) moves to a position where it supports ample production of available potential energy (APE) during the onset of the monsoon, c) the release of the available potential energy goes to enhance the kinetic energy of the irrotational component of the flow in the lower troposphere, d) the kinetic energy of the irrotational flow does not increase but is transferred rapidly to the corresponding non-divergent component of the flow via a number of interaction mechanisms and last but not the least e) orientation of irrotational and the non-divergent components of the flow field holds significant importance for the interaction and transfer mechanisms.

On the basis of these observational findings, Krishnamurti and Ramanathan (1982) conducted a series of numerical prediction experiments to examine the sensitivity of the monsoon onset to initially imposed irrotational flow fields. The results of these 96 h integrations revealed a large sensitivity in the evolution to the initial conditions of the flow field with regard to the orientation of the gradients of the velocity potential and the streamfunction fields.

The organization of convection refers to conversion of APE to eddy kinetic energy on the scale of

the disturbance. Like monsoon on the large-scale, tropical cyclones is another tropical phenomenon on much smaller spatio-temporal scales with very active convection that leads to strong generation of eddy kinetic energy. These two systems are very different in nature but have some basic relatable dynamical features such as both hurricanes and monsoons encounter organization of convection (or its disruption) during their life cycles and driven by organized deep convection. Organization of convection happens along a linear geometry for the monsoon onset isochrones whereas in tropical cyclones it occurs in a circular geometry.

Therefore, exploring these connections between Psi-Chi interaction and evolution of a tropical cyclone during its different stages would be an interesting aspect to explore. There are already several existing theories to explain tropical cyclogenesis. Here the objective is neither to support nor refute any of those theories but to provide a complimentary understanding for tropical cyclogenesis and its intensification.

1.1 Existing Theories of Evolution of Tropical Cyclones

The organization of systems at all scales has long been an observed feature in meteorology. Coherent structures can be found from eddies in the planetary boundary layer up to tropical cyclones and mid-latitude depressions. The problem of organization is thus of a fundamental nature. An understanding of the organization of deep convection is relevant to this general problem but is complicated by the three-phase physics of water. The phase changes play a fundamental role in convection, not only in producing hydrometeors, but in strongly influencing the internal dynamics through the buoyant force.

What is organization of convection? a) Convection that is long lived and generates circulation that initiates new cells and helps to maintain it, b) Covers an area larger than an individual

convective cell c) can be comprised of a group of cells in one cloud system (multicell) or a cluster of clouds d) formed by large-scale forcing, interaction with the large-scale flow, and/or by generating its own circulations that lead to upscale growth (self-organization)

Tropical cyclones which are a form of organized convection, extreme weather phenomena that have significant impacts on society. However, there remain significant gaps in our understanding of organization of convection in tropical cyclones, particularly how they form. There is no accepted theory for what controls the number of tropical cyclones. A tropical cyclone is a low pressure system (not associated with a front) that develops over tropical and sometimes sub-tropical waters and has organized deep convection with a closed wind circulation (generally 100-300 miles in diameter) about a well-defined center maintaining its identity for 24 hours. Tropical cyclogenesis often preceded by some disturbances or precursors, such as tropical easterly waves, African easterly waves, tropical upper tropospheric troughs and old frontal boundaries. Once a disturbance forms and is sustained, convection can develop it further and eventually evolve into a tropical depression in the presence of abundant supply of heat and moisture from the ocean with background cyclonic vorticity and weak wind shear.

Several necessary conditions for tropical cyclogenesis have been proposed by Riehl (1948), Gray (1968), and McBride and Zehr (1981) and define as follows:

1) A warm and large body of ocean water of at least 26.5°C throughout a sufficient depth of 50m (at least) to provide thermal energy for tropical cyclone.

2) Sufficient large planetary vorticity (at least a distance of 500 km from the equator so near gradient wind balance can occur)

3) A near surface preexisting disturbance with sufficient vorticity and convergence to generate low level converging wind triggering convection and helping to organize the mesoscale convective system

4) Divergence associated with an upper level trough overlaying the low level cyclonic disturbance to enhance the deep upward motion.

5) A potentially unstable atmosphere to allow the heat stored in the ocean to be released for the tropical cyclone development.

6) Relatively moist middle troposphere for allowing continuous development

7) Weak vertical wind shear with less than $10ms^{-1}$ between the ocean surface and the tropopause.

A tropical cyclone forms through complicated scale interaction between the small scale cumulus clouds, mesoscale organization of cumulus clouds and large scale environment. Organization of tropical cyclone formation is one of the most challenging problems in dynamic meteorology. Since the early 1960s several major mechanisms have been proposed to explain cyclogenesis. :- a) cooperative intensification mechanism b) linear CISK mechanism and c) WISHE mechanism.

1.1.1 Cooperative Intensification Mechanism

The cooperative intensification theory assumes that the broad-scale aspects of a tropical cyclone may be represented by an axisymmetric, balanced vortex in a stably- stratified, moist atmosphere. The basic mechanism was explained by Ooyama (1969) as follows.

In a weak cyclonic vortex there will be organized convective activity in the region where the frictionally induced inflow converges. The differential heating due to the organized convection introduces changes in the pressure field and that will generate a slow transverse circulation in the free atmosphere in order to reestablish the balance between the pressure and motion fields. If the equivalent potential temperature of the boundary layer is sufficiently high for the moist convection to be unstable, the transverse circulation in the lower layer will bring in more absolute angular momentum than is lost to the sea by surface friction. Then the resulting increase of cyclonic circulation in the lower layer and the corresponding reduction of the central pressure will cause the boundary-layer inflow to increase; thus, more intense convective activity will follow.

This mechanism assumes release of latent heat by moist convection given by the conditionally unstable moist air at the bottom of vertical column. The mechanism includes following process i) The heating effects of deep cumulus clouds are represented in terms of mass flux from the boundary layer to upper layer, ii) the deep cumuli will entrain ambient air from the middle layer as they rise through it and detrain in the upper layer iii) the entrainment rate is determined as a function of time to satisfy energy conservation and the air detrained into the upper layer follows the saturation equivalent potential temperature of ambient air in the layer.

1.1.2 Linear CISK Mechanism

A linear Conditional Instability of the second kind (CISK) mechanism has been proposed to explain tropical cyclogenesis (Charney and Eliassesn 1964) which includes the following processes i) the latent heat released by cumulus convection produces a lower tropospheric cyclonic disturbance in the environment ii) the disturbance will produce low level moisture convergence through boundary layer friction iii) low level convergence then lifts the conditionally unstable air

to the level of free convection and leads to the release of latent heat. In addition, the tropical atmosphere is assumed to be conditionally unstable. The essence of the theory is a positive feedback loop, where latent heat release caused by the large-scale circulation in turn reinforces it. Ekman pumping (vertical motion forced by horizontal frictional convergence) initiated from the large-scale vorticity field results in upward motion and latent heat release in the column. This forces the development of a secondary circulation and increased inward flow into the column. In turn, the vertical vortex is stretched, resulting in increased cyclonic vorticity at the surface and hence a greater amount of Ekman pumping.

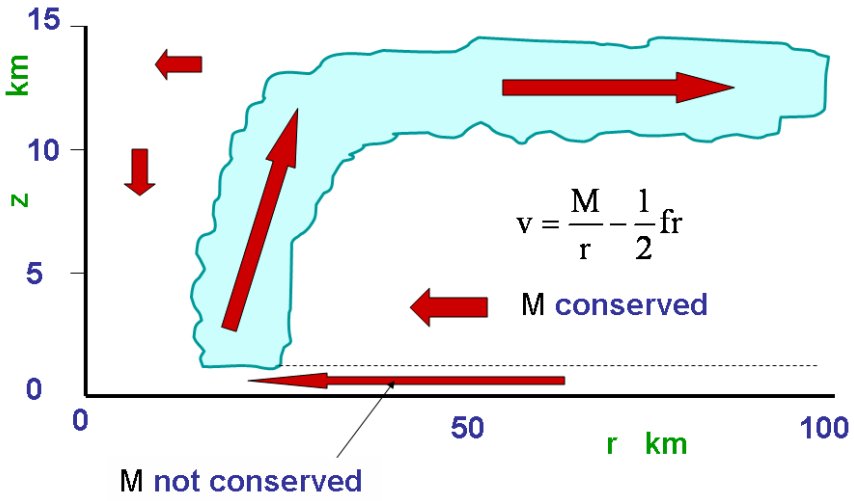

Figure1: Schematic of the axisymmetric view of tropical cyclone intensification in the rotating convection paradigm. Above the boundary layer, spin up of the vortex occurs as air parcels are drawn inwards by the inner-core convection. Air parcels spiraling inwards in the boundary layer may reach small radii quickly and acquire a larger tangential wind speed v (Montgomery et al. 2014).

Xu and Emanuel (1989) suggested that the key assumption of CISK, that the tropical atmosphere is generally conditionally unstable, is not right rather the atmosphere is near neutral to moist convective. Without a reservoir of convective available potential energy (CAPE), CISK could not exist. Another argument in CISK theory made by Charney and Eliassen, is that latent heating directly leads to kinetic energy production. Emanuel et al. (1994) argues that adiabatic cooling and radiative heat loss nearly offset the positive contribution of latent heat release, and that the correlation between heating and temperature is very difficult to determine.

1.1.3Wind Induced Surface Heat Exchange (WISHE)

Emanuel et al. (1994) presents the scenario of tropical cyclogenesis within a WISHE framework. It is based on the idea that the near surface wind speed in a tropical cyclone increases with decreasing radius. This increase is typically accompanied by an increase in near surface specific humidity, which leads to a negative radial gradient of equivalent potential temperature (θ_e) near the surface, and hence throughout the boundary layer.

An incipient vortex induces Ekman pumping, resulting in upward motion throughout the depth of the troposphere (assuming a length-scale of 500 km). Eventually, downdrafts result from this forcing, bringing low θ_e air into the sub cloud layer. Heat flux from the ocean surface initially is not enough to counteract this effect, and the vortex threatens to cool and spin down. The key factor that allows for amplification of the vortex is a moistening of the sub cloud layer to near saturation. Hence, when the moistened air is cycled into the secondary circulation, low θ_e air eventually disappears. This allows latent heat flux from the wind induced surface evaporation to begin to dominate, warming the core and allowing growth of the vortex. Thus, WISHE creates its own conditional instability through energy extraction from the ocean surface.

Air parcels in the inner core exit the boundary layer and rise upwards and ultimately outwards into the upper troposphere. As they do so, they conserve their M and θ_e values, carrying with them an imprint of the near surface radial gradients of M and θ_e into the interior of the vortex. Since the rising air rapidly saturates, the radial gradient of θ_e implies a negative radial gradient of virtual temperature. As air parcels move outwards conserving M they spin more slowly about the rotation axis of the storm, which, together with the positive radial gradient of M, explains the observed decrease of the tangential wind speed with height. But observations show that tropical cyclones are highly asymmetric during their intensification phase. Only the most intense storms exhibit a strong degree of axial symmetry and even then, only in their inner core region.

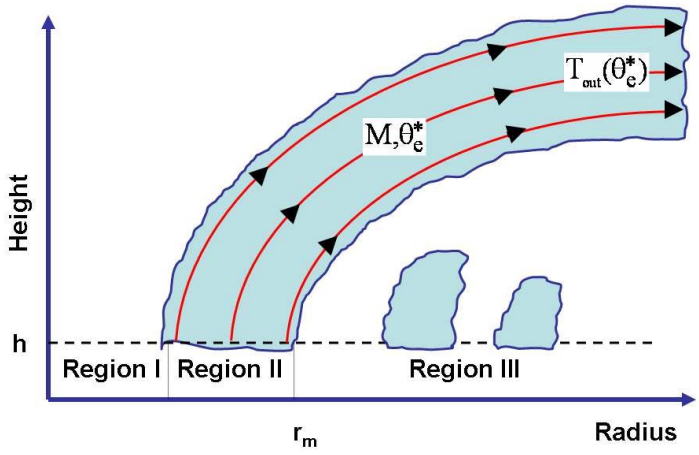

Figure 2.: Emanuel's 1986 model for a mature steady-state hurricane. The eye (Region I), the eyewall (Region II) and outside the eyewall (Region III). The absolute angular momentum per unit mass, M , and equivalent potential temperature, θ_e of an air parcel are conserved after the parcel leaves the boundary layer and ascends in the eye wall cloud. The model assumes that the radius of maximum tangential wind speed, r_m (Montgomery et al. 2014).

Observations show that rapidly developing storms with intense convection possess significant

amount of local buoyancy (Montgomery et al. 2009). The WISHE based developing hurricane contains neither cold downdrafts nor strongly buoyant updrafts, and no asymmetric convection. From this perspective, then, the WISHE theory appears incomplete and the question arises, what are its limitations? In an effort to address this question, Nguyen et al. (2008) carried out a series of high-resolution numerical experiments exhibiting a circularly symmetric, cloud-free, cyclonic initial vortex (at or below tropical storm strength), warm rain, pseudo adiabatic moist thermodynamics and a simple bulk formulation of the boundary layer including air-sea exchange processes (Montgomery et al. 2009).

In three dimensional tropical cyclone intensification, precipitation and evaporative cooling of warm rain processes are found to be dominated by highly localized deep convective structures possessing strong cyclonic vorticity in their cores. These vortical hot plume structures are known as vortical hot towers (VHT) (Hendricks et al., 2004; Montgomery et al., 2006). Here the intensification pathway is distinct from the WISHE, which requires a positive feedback between the boundary layer equivalent potential temperature and the surface wind speed underneath the eyewall of the storm.

The asymmetries in the vortex core are highly sensitive to the boundary layer moisture distribution. When a small random moisture perturbation is introduced in the boundary layer at the initial time, the pattern of the flow asymmetries changes dramatically causes a spread in azimuthal intensity change. When the moisture flux is suppressed altogether, there is no amplification of the system scale winds and the initial conditional available potential energy (CAPE) is rapidly consumed. The reason is that the pattern of convection is strongly influenced by the low-level moisture field (Nguyen et al. 2008, Shin and Smith 2008). Intensification from a finite-amplitude initial vortex is shown to not require this evaporation–wind feedback process. Indeed, when the surface wind

speed in the sea to air vapor fluxes is capped at a nominal (trade-wind) value, the vortex still intensifies by via the generation of locally buoyant VHTs and the near-surface convergence that the VHTs induce within the boundary layer.

CHAPTER 2

THEORY

2.1 Introduction to Psi-Chi Interaction

The stream function is defined for incompressible (divergence-free) flows in two dimensions as well as in three dimensions with axisymmetry. The flow velocity components can be expressed as the derivatives of the scalar stream function.

Consider a two-dimensional incompressible flow for which the continuity equation is given by

$$\frac{\partial u}{\partial x} + \frac{\partial v}{\partial y} = 0 \qquad (1)$$

A stream function is one which satisfies the eqn.1

$$\frac{\partial}{\partial x}\left(\frac{\partial \psi}{\partial y}\right) + \frac{\partial}{\partial y}\left(-\frac{\partial \psi}{\partial x}\right) \equiv 0 \qquad (2)$$

which then gives the components of the velocity vector in terms of streamfunction

$$u = \frac{\partial \psi}{\partial y}, \quad v = -\frac{\partial \psi}{\partial x} \qquad (3)$$

We can treat external flows around bodies as inviscid (i.e. frictionless) and irrotational (i.e. the fluid particles are not rotating). This is because the viscous effects are limited to a thin layer next to the body called the boundary layer. In this scenario We can define a potential function as a continuous function that satisfies the basic laws of fluid mechanics: conservation of mass and momentum, assuming incompressible, inviscid and irrotational flow.

By definition, for irrotational flow, $\nabla \times \vec{V} = 0$, So $\vec{V} = \nabla \phi$.

Therefore, velocity potential is given by $\phi = \phi(x, y, z, t)$.

Therefore, vector field in terms of velocity potential

$$u = \frac{\partial \phi}{\partial x}, \quad v = \frac{\partial \phi}{\partial y} \tag{4}$$

The horizontal wind vector and can be divided into two parts rotational and divergent so that

$$\vec{V}_H = \vec{V}_\psi + \vec{V}_\chi \tag{5}$$

It should be noted that Psi is the streamfunction and Chi is the velocity potential.

The rotational term can be defined as:-

$$\vec{V}_\psi = \vec{k} \times \nabla \psi \tag{6}$$

The divergent term can be defined as:-

$$\vec{V}_\chi = -\nabla \chi \tag{7}$$

Therefore, relative vorticity is defined as

$$\zeta = \vec{k} \cdot \nabla \times \vec{V}_H = \vec{k} \cdot \nabla \times \vec{V}_\psi = \nabla^2 \psi \tag{8}$$

The divergence is defined as

$$D = \nabla \cdot \vec{V}_H = \nabla \cdot \vec{V}_\chi = -\nabla^2 \chi \tag{9}$$

Given that total kinetic energy per unit mass is

$$K = \frac{1}{2}\vec{V}_H \cdot \vec{V}_H \tag{10}$$

It can be expanded to include the rotational and divergent winds yielding the following

$$\begin{aligned} K = \frac{1}{2}\vec{V}_H \cdot \vec{V}_H &= \frac{1}{2}(\vec{V}_\psi + \vec{V}_\chi) \cdot (\vec{V}_\psi + \vec{V}_\chi \\ &= \frac{1}{2}(\vec{V}_\psi \cdot \vec{V}_\psi) + \frac{1}{2}(\vec{V}_\chi \cdot \vec{V}_\chi) + \vec{V}_\psi \cdot \vec{V}_\chi \\ &= \frac{1}{2}|\nabla\psi|^2 + \frac{1}{2}|\nabla\chi|^2 - J(\psi,\chi) \end{aligned} \tag{11}$$

Note that the energy interaction between the rotational and divergent parts are represented by the Jacobian which satisfies the identity $J(\psi,\chi) \equiv \vec{k} \times \nabla\psi \cdot \nabla\chi$.

The kinetic energy due to non-divergent and irrotational parts are given by eqn. 12.

$$\begin{aligned} K_\psi &\equiv \frac{1}{2}|\nabla\psi|^2 \\ K_\chi &\equiv \frac{1}{2}|\nabla\chi|^2 \end{aligned} \tag{12}$$

$$K = K_\psi + K_\chi - J(\psi,\chi) \tag{13}$$

Therefore, the vorticity equation can be rewritten in terms of the stream function and the velocity potential

$$\begin{aligned} \frac{\partial}{\partial t}\nabla^2\psi &= -J(\psi, \nabla^2\psi + f) + \nabla\chi \cdot \nabla(\nabla^2\psi + f) - \omega\frac{\partial}{\partial p}\nabla^2\psi \\ &+ (\nabla^2\psi + f)\nabla^2\chi - \nabla\omega \cdot \nabla\frac{\partial\psi}{\partial p} + J\left(\omega, \frac{\partial\chi}{\partial p}\right) + F_\zeta \end{aligned} \tag{14}$$

The divergence equation can also be rewritten in terms of the streamfunction and the velocity potential

$$\frac{\partial}{\partial t}\nabla^2\chi = \nabla^2\left[\frac{1}{2}(\nabla\psi)^2 + \frac{1}{2}(\nabla\chi)^2 - J(\psi,\chi)\right] - (\nabla^2\psi)^2 - \nabla\psi\cdot\nabla(\nabla^2\psi)$$
$$-\omega\frac{\partial}{\partial p}\nabla^2\chi - J\left(\omega,\frac{\partial\psi}{\partial p}\right) - \nabla\omega\cdot\nabla\frac{\partial\chi}{\partial p} - \nabla f\cdot\nabla\psi$$
$$+ J(f,\chi) + J(\nabla^2\psi,\chi) + f\nabla^2\psi + \nabla^2\phi + F_D \qquad (15)$$

The following identities should also be noted

$$\psi\frac{\partial}{\partial t}\nabla^2\psi = \nabla\cdot\left(\psi\nabla\frac{\partial\psi}{\partial t}\right) - \frac{\partial}{\partial t}\left(\frac{|\nabla\psi|^2}{2}\right) \qquad (16)$$

$$\chi\frac{\partial}{\partial t}\nabla^2\chi = \nabla\cdot\left(\chi\nabla\frac{\partial\chi}{\partial t}\right) - \frac{\partial}{\partial t}\left(\frac{|\nabla\chi|^2}{2}\right) \qquad (17)$$

Based on the definitions from (12) the above equations can be written as

$$\frac{\partial}{\partial t}K_\psi = -\psi\frac{\partial}{\partial t}\nabla^2\psi + \nabla\cdot\left(\psi\nabla\frac{\partial\psi}{\partial t}\right) \qquad (18)$$

$$\frac{\partial}{\partial t}K_\chi = -\chi\frac{\partial}{\partial t}\nabla^2\chi + \nabla\cdot\left(\chi\nabla\frac{\partial\chi}{\partial t}\right) \qquad (19)$$

For simplicity many of the terms in the energy equation will be expressed in the form of a divergence of a vector or a Jacobian of two scalars, so that the integration of the energy equation over a closed domain will allow those terms to vanish. By multiplying (14) by ψ and (15) by χ the

following equations are obtained:

$$\psi \frac{\partial}{\partial t}\nabla^2\psi = -\psi J(\psi, \nabla^2\psi + f) + \psi\nabla\chi\cdot\nabla(\nabla^2\psi + f) - \psi\omega\frac{\partial}{\partial p}\nabla^2\psi$$
$$+\psi(\nabla^2\psi + f)\nabla^2\chi - \psi\nabla\omega\cdot\nabla\frac{\partial\psi}{\partial p} + \psi J\left(\omega, \frac{\partial\chi}{\partial p}\right) + F_\psi \tag{20}$$

$$\chi\frac{\partial}{\partial t}\nabla^2\chi = \chi\nabla^2\left[\frac{1}{2}(\nabla\psi)^2 + \frac{1}{2}(\nabla\chi)^2 - J(\psi,\chi)\right] - \chi(\nabla^2\psi)^2$$
$$-\chi\nabla\psi\cdot\nabla(\nabla^2\psi) - \chi\omega\frac{\partial}{\partial p}\nabla^2\chi - \chi J\left(\omega, \frac{\partial\psi}{\partial p}\right) - \chi\nabla\omega\cdot\nabla\frac{\partial\chi}{\partial p} - \chi\nabla f\cdot\nabla\psi$$
$$+\chi J(f,\chi) + \chi J(\nabla^2\psi,\chi) + \chi f\nabla^2\psi + \chi\nabla^2\phi + F_\chi \tag{21}$$

where $F_\psi = \psi F_\zeta$ and $F_\chi = \chi F_D$

In eqn. 20 terms on the right side can be rearranged as follows:

$$-\psi J(\psi, \nabla^2\psi + f) = -J\left(\frac{\psi^2}{2}, \nabla^2\psi + f\right) \tag{22}$$

$$= -\psi\nabla\cdot\left(\omega\nabla\frac{\partial\psi}{\partial p}\right)$$
$$= -\nabla\cdot\left(\psi\omega\nabla\frac{\partial\psi}{\partial p}\right) + \omega\nabla\psi\cdot\nabla\frac{\partial\psi}{\partial p}$$
$$= -\nabla\cdot\left(\psi\omega\nabla\frac{\partial\psi}{\partial p}\right) + \omega\frac{\partial}{\partial p}\frac{|\nabla\psi|^2}{2}$$
$$= -\nabla\cdot\left(\psi\omega\nabla\frac{\partial\psi}{\partial p}\right) + \frac{\partial}{\partial p}\frac{\omega|\nabla\psi|^2}{2} - \frac{|\nabla\psi|^2}{2}\frac{\partial\omega}{\partial p}$$
$$= -\nabla\cdot\left(\psi\omega\nabla\frac{\partial\psi}{\partial p}\right) + \frac{\partial}{\partial p}\frac{\omega|\nabla\psi|^2}{2} - \frac{|\nabla\psi|^2}{2}\nabla^2\chi$$

$$-\psi\nabla\omega\cdot\nabla\frac{\partial\psi}{\partial p} - \psi\omega\frac{\partial}{\partial p}\nabla^2\psi = -\psi\left[\nabla\cdot\left(\omega\nabla\frac{\partial\psi}{\partial p}\right) - \omega\nabla^2\frac{\partial\psi}{\partial p}\right] - \psi\omega\frac{\partial}{\partial p}\nabla^2\psi \tag{23}$$

Now,

$$\psi\nabla\chi\cdot\nabla\left(\nabla^2\psi+f\right)+\psi\left(\nabla^2\psi+f\right)\nabla^2\chi$$

$$\begin{aligned}
&=\psi\nabla\chi\cdot\nabla\left(\nabla^2\psi\right)+\psi\nabla\chi\cdot\nabla f+\psi\nabla^2\psi\nabla^2\chi+\psi f\nabla^2\chi\\
&=\nabla\cdot\left(\psi\nabla^2\psi\nabla\chi\right)-\nabla^2\psi\nabla\psi\cdot\nabla\chi-\psi\nabla^2\psi\nabla^2\chi+\psi\nabla^2\psi\nabla^2\chi\\
&+\nabla\cdot\left(\psi f\nabla\chi\right)-\nabla\psi\cdot f\nabla\chi+\psi f\nabla^2\chi\\
&=\nabla\cdot\left(\psi\nabla^2\psi\nabla\chi\right)-\nabla^2\psi\nabla\psi\cdot\nabla\chi+\nabla\cdot\left(\psi f\nabla\chi\right)-\nabla\psi\cdot f\nabla\chi+\psi f\nabla^2\chi
\end{aligned}\tag{24}$$

$$\psi J\left(\omega,\frac{\partial\chi}{\partial p}\right)=J\left(\omega\psi,\frac{\partial\chi}{\partial p}\right)-\omega J\left(\psi,\frac{\partial\chi}{\partial p}\right)\tag{25}$$

Substituting equations (22) through (25) into equation (20) and integrating over a closed domain yields the rotational kinetic energy equation (Psi-Chi interaction equation) used for this study.

$$\frac{\partial}{\partial t}\overline{\overline{K_\psi}}=\overline{\overline{f\nabla\psi\cdot\nabla\chi}}+\overline{\overline{\nabla^2\psi\nabla\psi\cdot\nabla\chi}}+\overline{\overline{\nabla^2\chi\frac{|\nabla\psi|^2}{2}}}+\overline{\overline{\omega J\left(\psi,\frac{\partial\chi}{\partial p}\right)}}+\overline{\overline{F_\psi}}\tag{26}$$

Now the Thermodynamic equation is:-

$$s=C_pT-\alpha=C_p\frac{\partial T}{\partial p}+\frac{\partial\phi}{\partial p}\tag{27}$$

$$\begin{aligned}
-\omega s&=-\omega\frac{\partial}{\partial p}\left(C_pT+\phi\right)\\
&=-\frac{\partial}{\partial p}\left[\omega\left(C_pT+\phi\right)\right]+\left(C_pT+\phi\right)\frac{\partial}{\partial p}\omega\\
&=-\frac{\partial}{\partial p}\left[\omega\left(C_pT+\phi\right)\right]+\left(C_pT+\phi\right)\nabla^2\chi
\end{aligned}\tag{28}$$

Integrating the thermodynamic equation over a closed domain gives

$$\overline{\overline{APE}} = \overline{\overline{\chi \nabla^2 \phi}} \tag{29}$$

Consider that in the absence of diabatic heating and friction, the total energy is conserved, i.e.,

$$\frac{\partial}{\partial t}\overline{\overline{APE + K}} = \frac{\partial}{\partial t}\overline{\overline{APE + K_\psi + K_\chi}} = 0 \tag{30}$$

Hence,

$$\begin{aligned}\frac{\partial}{\partial t}\overline{\overline{K_\chi}} &= -\frac{\partial}{\partial t}\overline{\overline{APE}} - \frac{\partial}{\partial t}\overline{\overline{K_\chi}} \\ &= -\overline{\overline{\chi \nabla^2 \phi}} - \overline{\overline{f \nabla\psi \cdot \nabla\chi}} - \overline{\overline{\nabla^2\psi(\nabla\psi \cdot \nabla\chi)}} \\ &\quad - \overline{\overline{\frac{1}{2}|\nabla\psi|^2 \nabla^2\chi}} - \overline{\overline{\omega J\left(\psi, \frac{\partial\chi}{\partial p}\right)}} + \overline{\overline{F_\chi}}\end{aligned} \tag{31}$$

Eqn. 26, 30 and 31 gives rate of change of non divergent, irrotational and APE.

Finally, we are here interested on two equations:

Conversion of divergent to rotational kinetic energy

$$\frac{\partial \bar{\bar{K}}_\psi}{\partial t} = \underbrace{\overline{\overline{f \nabla\psi . \nabla\chi}}}_{Term\ 1} + \underbrace{\overline{\overline{\nabla^2\psi \nabla\psi . \nabla\chi}}}_{Term\ 2} + \underbrace{\overline{\overline{\nabla^2\chi\left(\frac{\nabla\psi}{2}\right)^2}}}_{Term\ 3} + \underbrace{\overline{\overline{\omega J\left(\psi, \frac{\partial\psi}{\partial p}\right)}}}_{Term\ 4} + \bar{\bar{F}}_\psi + B_\psi \ldots\ldots\ldots\ldots\ldots\ldots (32)$$

(33)

$$\frac{\partial \bar{\bar{K}}_\chi}{\partial t} = -\underbrace{\overline{\overline{f \nabla\psi . \nabla\chi}}}_{Term\ 1} - \underbrace{\overline{\overline{\nabla^2\psi \nabla\psi . \nabla\chi}}}_{Term\ 2} - \underbrace{\overline{\overline{\nabla^2\chi\left(\frac{\nabla\psi}{2}\right)^2}}}_{Term\ 3} - \underbrace{\overline{\overline{\omega J\left(\psi, \frac{\partial\psi}{\partial p}\right)}}}_{Term\ 4} - \underbrace{\overline{\overline{\chi \nabla^2 \emptyset}}}_{Term\ 5} + \bar{\bar{F}}_\chi + B_\chi \ldots\ldots\ldots (33)$$

Conversion of available potential to divergent kinetic energy

$$\overline{\overline{< APE \cdot K_\chi >}} = -\overline{\overline{\chi \nabla^2 \phi}} \tag{34}$$

Final form of equation 32. Also can be written

$$\overline{\overline{< K_\chi \cdot K_\psi >}} \equiv \overline{\overline{f \nabla\psi \cdot \nabla\chi}} + \overline{\overline{\nabla^2\psi \nabla\psi \cdot \nabla\chi}} + \overline{\overline{\nabla^2\chi \frac{|\nabla\psi|^2}{2}}} + \overline{\overline{\omega J\left(\psi, \frac{\partial\chi}{\partial p}\right)}} \tag{35}$$

2.2 Proposed Theory for Relation Between PSI-CHI Interaction and Evolution of tropical cyclone

Evolution of any convective system is the conversion of available potential energy to eddy kinetic energy on the scales of convection (Krishnamurti and Ramanathan 1982). The domain averaged energy transfers from the irrotational to the non-divergent component of the motion field. Psi-Chi framework would allow one to follow the flow of energy from anomalous generation of available potential energy through the thermal efficiency exchange to the primary psi-chi exchange, and that the dot product in the primary psi-chi exchange would have consequences on the non divergent kinetic energy. The first idea is that the available potential energy can only be converted to and from the kinetic energy of the irrorational component of the wind (Krishnamurti et al. 1997). Diabatic heating (i.e., the covariance of heating and temperature) leads to the growth of available potential energy in a tropical cyclone, which is passed on to the divergent motions via the covariance of vertical velocity and temperature (Lin and smith 1979).

Term 1. $\overline{\overline{f \nabla\psi \cdot \nabla\chi}}$

Term 2. $\overline{\overline{\nabla^2\psi\nabla\psi\cdot\nabla\chi}}$

Term 3. $\overline{\overline{\nabla^2\chi\frac{|\nabla\psi|^2}{2}}}$

Term 4. $\overline{\overline{\omega J\left(\psi,\frac{\partial\chi}{\partial p}\right)}}$

Term 5. $\overline{\overline{\frac{R}{p}\omega T}}$

The Terms 1, 2, 3, and 4 of Equations X and Y are the $\psi-\chi$ energy interaction terms, which represent the contributions from the orientation of the gradients of the ψ and χ, the orientation of the gradients of ψ and χ in the vicinity of the vorticity, the covariance of the horizontal divergence and the kinetic energy of the non-divergent component, respectively. All of these Terms (1 through 4) appear as a source and as a sink (with an opposite sign) in Equations 1 and 2. The magnitude of Term 1, as it is a dot product of two vectors critically depends on the orientation of the gradients of ψ and χ and the magnitude of the gradients. In the northern hemisphere, if the two vectors are oriented parallel then the dot product will be maximized. This Term 1 represents the interaction of the large-scale ψ and χ fields of the TC environment. In contrast, Term 2 represents the same interaction as Term 1 but in the vicinity of the cyclonic vorticity (in the northern hemisphere) TCs. It is evident from the expression of Term 3 that it can lead to exponential growth of non-divergent kinetic energy in the presence of strong convergence in the northern hemisphere. Term 4 represents interaction between K_ψ and K_χ in the presence of

strong vertical gradients of convergence. This term is at least an order of magnitude smaller than the other three terms both at 850hPa and in the outflow level and is therefore not discussed.

Term 5 is unique to Equation 31, which does not appear in Equation 32. It represents Available Potential Energy (APE) and serves as the source for the interaction between $K_\psi \; and \; K_\chi$. Krishnamurthi and Ramanathan (1982) show that this term can also be written as: $\overline{\overline{\frac{R}{p}\omega T}}$, where, ω and T are omega and temperature, respectively. APE can therefore be interpreted as a covariance of the vertical motion with temperature that denotes the ascent of warm air and descent of cold air within the domain. If diabatic processes in a TC generate APE this can be converted to kinetic energy in the secondary circulation via buoyancy fluxes, and then in turn to kinetic energy in the primary circulation, resulting in vortex formation at an early stage and later intensification as well.

As Krishnamurti and Ramanathan (1982) found in the evolution of the Indian summer monsoon, we envisage the energy transfer from condensational heating in the convective clouds of the TC to its non-divergent component of the winds through the irrotational component of the flow. The intent of this paper is not to compute an energy budget but to understand the interaction of the irrotational and non-divergent components of the wind in a TC and potentially shed light on the evolution of the intensity of the TC in this framework of $\psi - \chi$ interaction. The friction terms, $\bar{\bar{F}}_\psi$ and $\bar{\bar{F}}_\chi$ and the boundary flux terms B_ψ and B_χ appearing in Equations 1 and 2 are not computed in this study as the remaining terms in Equations 1 and 2 are able to clearly discern the diverse evolution of the three cases. Moreover, the intent here is not to compute an energy budget.

All tropical cyclones are characterized by an incipient low pressure system that grows over the period of simulation and second period a time when the cyclonic circulation further intensified

to attain tropical cyclone status. So these two time periods of evolution of tropical storm Cindy provide an opportunity to contrast their psi-chi interactions.

Neglecting boundary fluxes, the non divergent flow can only gain energy at the expense of the divergent flow. The interaction between irrotational and non divergent component of the wind flow is a necessary condition for organization of a convective activity i.e. generation of a system, maintenance over a sustainable amount of time and then getting to stage of intensification.

In Psi-Chi exchange equation (eqn.32) the first term involving the Coriolis parameter and the second term involving relative vorticity, are the most important. A simple scale analysis will reveal that in a tropical cyclone environment that these two terms are an order of magnitude higher than all other terms in eqn. 32. Even without doing any analysis it can be said that organization of convection in a circular pattern will have higher relative vorticity so Term 2 has the potential to determine whether a system will turn into tropical cyclone or not. Term 1 will also be of equal interest as mostly we are talking about a system which requires Coriolis fore as steering factor for the production of cyclonic circulation and also because the region of interest lies between 10^0N and 32^0N which is away from tropics. As the system will continue to move northward Term 1 will increase. So for evolution of tropical cyclone Term 1 and Term 2 would be critical as well Term 3 which is convergence of nondivergent energy. It is expected that nondivergent kinetic energy continues to grow with time, for both the periods of genesis and intensification an environmental prerequisite is formation of rotational kinetic energy. During genesis the system will move from a background of no rotational kinetic energy to a place which is supportive to any closed circulation whereas during intensification period individual terms will grow from a pre existing lower value to a higher value.

Vector orientation differs from parallel to perpendicular to antiparallel, based on angle between them (discussed in previous section). Vector orientation controls the evolution of kinetic energy due to non divergent field i.e. the psi-chi interaction and the angle controls the magnitude of individual terms.When the angles are between the range of 0-90 then the dot product (mentioned in previous figures) will have positive values which is favorable for psi-chi interaction and in turn will help organization of convection. Whereas angle ranging between 90-180 will create exactly opposite scenario and hinder the process of genesis. We understand from dynamical point of view that there must be a difference in the strength of non divergent kinetic energy represented by Term1, Term2 and Term3 but the question comes that why is there any such potential difference at those two stages or storms of different strength? The answer lies in the computation of angle between gradient of stream function and gradient of velocity potential and represented by θ.

Θ can be computed by following equation.

$$\Theta = \cos^{-1} [\nabla\Psi.\nabla\boldsymbol{\chi}/\{abs(\nabla\Psi)\ abs\ (\nabla\boldsymbol{\chi}\ )\}] \qquad (36)$$

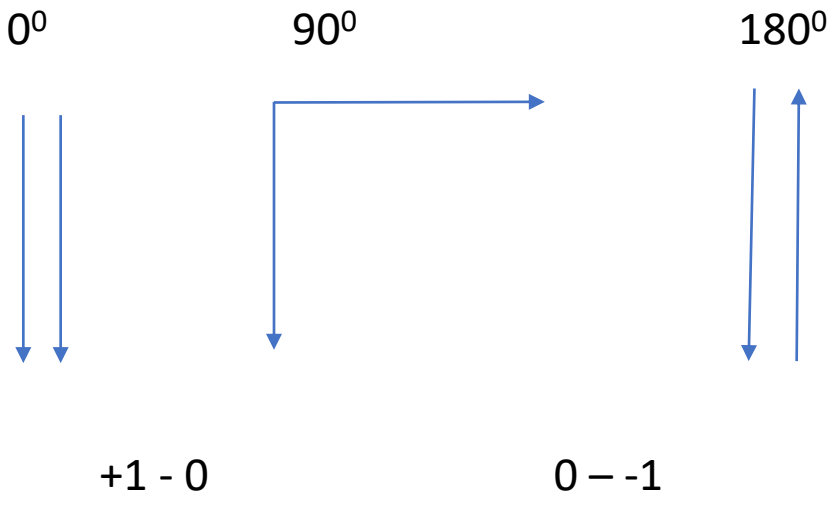

Figure 3. 1 represents the maximum value of the cosine function and -1 minimum value

$Cos^{-1}\theta$ is restricted to 0 – 180 degree as well θ. So it can be assumed when the angle lies between 0^0-90^0 cosine of θ corresponds to positive value of $\nabla\Psi.\nabla\boldsymbol{\chi}$ which implies generation of Term 1 and term 2 but when θ changes to a range of 90^0-180^0 cosine value becomes negative and so the $\nabla\Psi.\nabla\boldsymbol{\chi}$ and eventually there is destruction of non divergent component happens. So for organization convection across a low pressure system entails an atmosphere of strong positive values of $\nabla\Psi.\nabla\boldsymbol{\chi}$. Not only the sign but value of angle determines strength of the dot product which in turn controls the amount non divergent kinetic energy production at two stages of organization. Angle between the vectors also signifies their orientation to one another. As angle grows 0-90 vectors become parallel to orthogonal, further growth make the vectors anti-parallel which is not conducive to growth of any convective system. So in other word when the vectors are parallel to each other they promote organization of convection.

CHAPTER 3

METHODOLOGY

3.1Background

3.1.1NASA Convective Processes Experiment (CPEX)

The NASA Convective Processes Experiment (CPEX) aircraft field campaign took place in the North Atlantic-Gulf of Mexico-Caribbean Ocean region during the early summer of 2017. This campaign collected data to help answer questions about convective storm initiation, organization, growth, and dissipation. For this effort, NASA's DC-8 aircraft flew for 100 hours of flight time and equipped with multiple instruments capable of taking measurements that will help scientists improve their understanding of convective processes. For the first time on a single research aircraft, the DC-8 had a suite of instruments with the capability of detailed wind, temperature, and humidity profiles beneath the aircraft at horizontal resolution of a few kilometers, potentially enabling CPEX scientists to obtain essential details of atmospheric structure, together with dual-frequency Doppler radar data for determining the structure of storms, to observe the evolution of convective storm systems together with their evolving environment.

The current work is in support of the NASA sponsored Convective Process Experiment (CPEX). The overarching purpose of CPEX is to better understand the convective processes that leads to hurricane formation (or dissipation), which will lead to improved forecasting including hurricane track and intensity prediction. CPEX is a science-driven, hypothesis-based approach to understand what leads to convective initiation and the role played by the environment in organizing convection.

Most tropical disturbances, such as hurricanes need organization of convection during their life cycles of intensification. A major, unsolved, scientific problem is that related to the understanding of the factors responsible for the organization, or in many cases the disruption, of the convection process. Organized deep convection in a near circular geometry provides generation of available potential energy, and enables its transformation to kinetic energy on the same scales as that of the organization of convection. CPEX builds upon a substantial foundation towards improving the understanding of the life cycle of hurricane from the use of observations and modeling. We propose to address specifically the relationship of the organization of convection with the kinematics (or wind field changes). Main objectives of our work is to evaluate the effects of ambient conditions on the organization or disruption of convection,

The convection processes of hurricanes are influenced by numerous atmospheric and oceanic factors, including aerosols, wind shear, dry air incursions, oceanic warm and cold thermal anomalies and extra-tropical influences. These factors dictate whether convection is organized or disrupted, leading to the formation or dissipation of hurricane. CPEX studies these major influences to understand the resultant intensity and motion of such storms. Alternatively, the organization of convection in a hurricane can also be influenced by the gradients in the wind field, especially in the tropics where geostrophy is weak and mass and wind relationships are not tied by any known relationships. Wind observations are a major limitation in observational and modeling studies of these phenomena, which often occur in the open oceans especially at the time of their genesis. This limitation is directly addressed by CPEX, which utilizes 3-D winds obtained from DAWN, temperatures moisture, aerosol profiling, and radar observations through observing platforms fitted into a DC-8 plane that was flown through these specific weather events in June 2017.

3.1.2Tropical Cyclone Cindy (2017)

The 2017 Atlantic hurricane season was an active and catastrophic hurricane season with four hurricanes making landfall (Harvey as Cat 4, Irma as Cat 4, Maria as Cat 4 and Nate as Cat 1). The 2017 season saw a total of 17 named storms, with ten of these storms reaching hurricane strength. In mid June, two tropical waves and an area of disturbed weather began merging over the western Caribbean Sea. A low pressure region began to organize from a tropical disturbance on June 16, 2017 in the western Caribbean Sea near the coast of Nicaragua and Honduras. The area of low pressure continued to move northwest towards the Yucatan Peninsula throughout the weekend and into Monday, June 19. On Monday (June 19) afternoon, the low pressure emerged into the southern Gulf of Mexico and the National Hurricane Center (NHC) designated the system as Potential Tropical Cyclone #3 as it became more organized. The Gulf disturbance was expected to become a tropical depression or Tropical Storm shortly as it was situated over an area that is quite favorable for development in June, where many past June tropical storms have formed. The disturbance moved slowly northwestward and on June 20th, the system gained tropical storm strength and became Tropical storm Cindy with max sustained winds of 45mph. Cindy developed within a large Central American cyclonic gyre, which was likely induced by the positive phase of the Madden-Julian Oscillation during the second week of June and then subsequently enhanced by the passage of two consecutive tropical waves. The first tropical wave moved off the west coast of Africa on 4 June and eventually contributed to a northward influx of moisture near Central America on 14–15 June. The following tropical wave, which initially moved off the west coast of Africa on 7 June, caught up with to this area of disturbed weather over the far western Caribbean Sea on 17 June. The vorticity associated with the second wave moved northwestward across the northwestern Caribbean Sea and Yucatan Peninsula within the Central American gyre, reaching

the south-central Gulf of Mexico on 19 June. Even though a broad area of low pressure had developed by that time and was already producing gale-force winds east of the surface trough, the system did not have a well-defined center, and the low-level circulation was elongated with multiple embedded swirls. In addition, a large but linear band of deep convection extended east of the trough axis over the eastern Gulf of Mexico. The next day, the multiple low-level swirls consolidated into a sufficiently well-defined center of circulation, and deep convection showed increasing curvature around the new center. As a result, a tropical storm formed over the central Gulf of Mexico by 1800 UTC 20 June.

It is quite evident that though tropical cyclone Cindy was named on 20th June but it had a conducive environment for genesis since 17th June over the Caribbean for the development of a depression which later moved to GoM. So if we consider the whole time period then there are two periods with distinct large scale features helpful to understand organization of convection during its initiation phase and slow intensification period after it attained tropical storm status. Our primary goal is to unveil the dynamical process involved during organization of convection in terms of interaction between wind components within the vortex and its environment. Cindy is a perfect selection to fulfill the goal of the current study. Large scale condition indicates a favorable phase during 17th June 0000UTC – 19th June 0000UTC over the Caribbean region. By 19th June low level circulation with precipitation reaching north GoM through Yucatan channel. The next phase i.e. between 19th June 0600UTC – 21st June 0600UTC involves movement over GoM, slow intensification and translation into a tropical cyclone. This phase was characterized by broad low pressure extending from Yucatan to SE GoM and winds were easterly and south easterly. There was advection of moisture from the Caribbean and as well as from east Pacific. Eventually low pressure moved into central GoM with increasing surface winds and shear was reduced over central

GoM but strong north of 26N.South easterly winds were advecting moisture from Caribbean but by 21st June advection of moisture had been reduced.

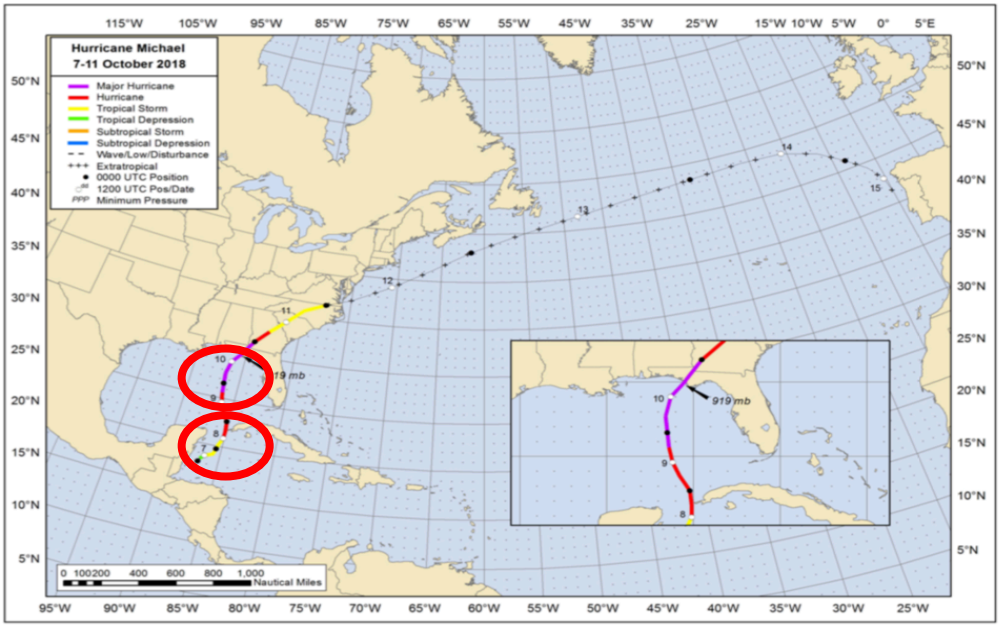

Figure 4. Path of tropical cyclone Cindy (2017). Two red circles marking the simulation periods (described later).

3.1.3 Tropical cyclone Irma 2017

Irma which was first Category 5 Atlantic hurricane of 2017 tropical cyclone season sustained for a very long time and caused severe damage starting from the Caribbean islands to the Florida Keys. On 27th August a Cape Verde tropical wave created a deep convection which became stronger in following two days. By 30th August the convection turned into a tropical depression and at precisely 0600 UTC of the same day it was named tropical storm. It continued to move westward under the impact of eastern Atlantic mid-level ridge. All the key ingredients necessary for rapid intensification of tropical storms such as warm SST, moist lower troposphere and weak vertical wind shear were present, which helped Irma to strengthen and by 0000 UTC 31st August it had a

prominent eye. 1st September 0000 UTC, Irma's maximum wind speed reached 100 kts. Between 1st September and 4th September Irma's intensity reduced from Category 3 to Category 2 and underwent an Eyewall Replacement Cycle (ERC). By early 4th September with the completion of ERC, Irma started strengthening again and attained maximum wind speed of 155kts by1800 UTC of 5th September, while it continued to move west north-westward. On 0545 UTC 6th September Irma made its first landfall at Barbuda island as Category 5 hurricane. Our model simulation of this TC spanned a 48 hour period ending 0000UTC of 6 September.

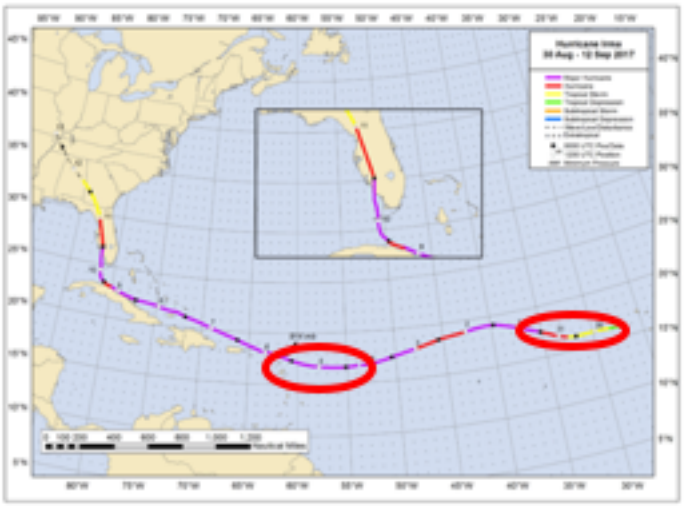

Figure 5. Path of tropical cyclone Irma (2017). Two red circles marking the simulation periods (described later).

3.1.3 Tropical cyclone Michael 2018

Hurricane Michael (2018) was a Gulf of Mexico Category 5 hurricane that made landfall near Panama City, Florida. Michael initially originated from a wide spread low pressure system near southwestern Caribbean Sea. From its incipient stage on 1st October it evolved to be a named tropical cyclone on 7th October. Michael had a unique genesis scenario. A convective burst in

association with a tropical wave led to the formation of low pressure near Jamaica on 2nd October and moved to west-southwestward, reached northwest Honduras by 4th October. Later the low pressure system, which was surrounded by a large cyclonic gyre over Central America, created an inland vorticity center on 6th October near extreme eastern Pacific Ocean and eventually absorbed by the gyre while moving inland central America, center reformed over north western Caribbean forming a tropical depression by 0600 UTC of 7th October. Within 6 -12 hours of the genesis, the system reformed and moved north north-westward under the influence of the mid-level ridge over western Atlantic. Despite the presence of southwesterly wind shear by an upper level trough the depression rapidly intensified and became a tropical cyclone in the next 6 hours from genesis and eventually by 1200UTC of 8th October transitioned into a hurricane and continued to get stronger. The rapid intensification was due to diffluence caused by the trough. Shear, dry air intrusion caused a halt in Michael's intensification in southeastern Gulf of Mexico around 1200 UTC of 8th October. But this situation changed quickly and the hurricane again rapidly intensified. The maximum sustained wind reached its peak of 145 kts around 1730 UTC of 10th October just before it made landfall. Our model simulation spanned a 48 hour period of this TC ending at 1800UTC of 10 October.

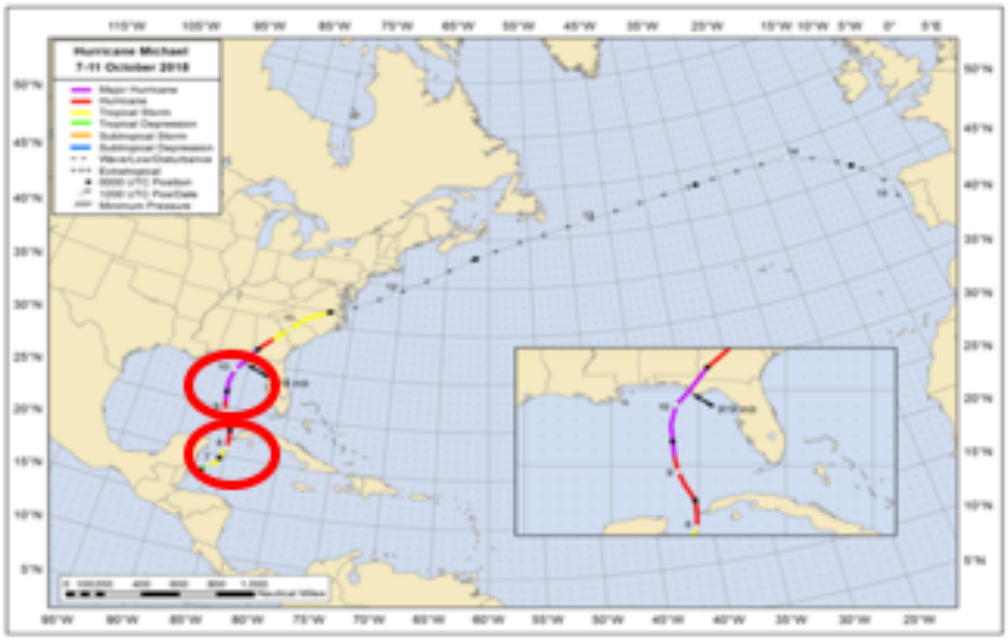

Figure 6. Path of tropical cyclone Michael (2018). Two red circles marking the simulation periods (described later).

3.2 Design of Experiments

3.2.1 Model Selection

WRF is a next-generation, mesoscale numerical weather prediction system featuring multiple dynamic cores designed to serve both operational forecast and research needs (Skamarock et al. 2005). It is based on an Eulerian solver for the fully compressible non-hydrostatic equations, cast in flux conservation form, using a mass (hydrostatic pressure) vertical coordinate. The solver uses a third-order Runge–Kutta time integration scheme coupled with a split-explicit second order time integration scheme for the acoustic and gravity wave modes. Fifth-order upwind biased advection operations are used in the fully conservative flux divergence integration; second- to sixth-order schemes are run-time selectable. WRF has multiple physical options for cumulus, microphysics,

planetary boundary layer, and radiation physical processes. Details of the model are provided in. The weather research and forecasting model (WRF) version 3.8.1 was used for the simulation. WRF is widely used for both research and operational weather forecasting in the mid- latitudes, tropics, and for tropical cyclones. Many recent studies have shown that, with sufficient horizontal and vertical resolution, WRF is capable of reproducing many features of hurricanes with reliability [Davis et al., 2008; Nolan et al., 2009a, 2009b; Lee and Chen, 2012].

For this study, WRF has a domain resolution of 3-km grid spacing with model vertical structure comprises 37 σ levels with the top of the model set at 100 hPa, where σ = (ph − pht)/(phs − pht), while ph is the hydrostatic component of the pressure, and phs and pht refer to values of the pressure along the surface and top boundaries, respectively. The σ levels are placed close together in the low levels (below 500 hPa) and are relatively coarsely spaced above. The model was initialized by The NCEP operational Global Forecast System (GFS) data on a 0.25 by 0.25 global latitude longitude grid. The NCEP GFS include analysis time steps at a 3 hourly interval from 0 to 48 hrs.

3.2.2 Selection of Model Microphysics

Numerous physical processes in the atmosphere occur on scales smaller than can be resolved by the model. These include the formation of clouds and precipitation (microphysics), the transmission and absorption of solar and infrared radiation, and the vertical and horizontal mixing of momentum and scalars by turbulence. Figure 1. shows that within the model there is an interaction and feedback mechanism among microphysics, cumulus. radiation, PBL and surface schemes. There is direct or indirect effect of one scheme to the other and changing one particular criterion will influence their interaction. Here, for this study emphasis is given on microphysical

processes and two of them have been specifically selected. In our preliminary simulations the WRF 6 class single-moment scheme (WSM6) (MP1) [Hong and Lim, 2006] and Kessler scheme (MP2) have been used and compared. It has been found that the single-moment scheme (WSM6) produced more realistic distributions of precipitation, with smaller areas of very high intensity, and broader areas of light precipitation. Microphysics processes control the simulation of the formation of cloud droplets, the formation of ice crystals, their growth, and their fallout as precipitation. The key role for it on cloud, climate and weather models can be shown in (1) Latent heating/cooling: condensation, evaporation, deposition, sublimation, freezing, melting (2) Condensate loading: (mass of the condensate carried by the flow) (3) Precipitation: fallout of larger particles. (4) Coupling with surface processes: moist downdrafts leading to surface-wind gustiness, cloud shading. (5) Radiative transfer: mostly total mass of the water species that modulates absorption/emission of long wave, particle size of the water species is also important for short wave radiation.

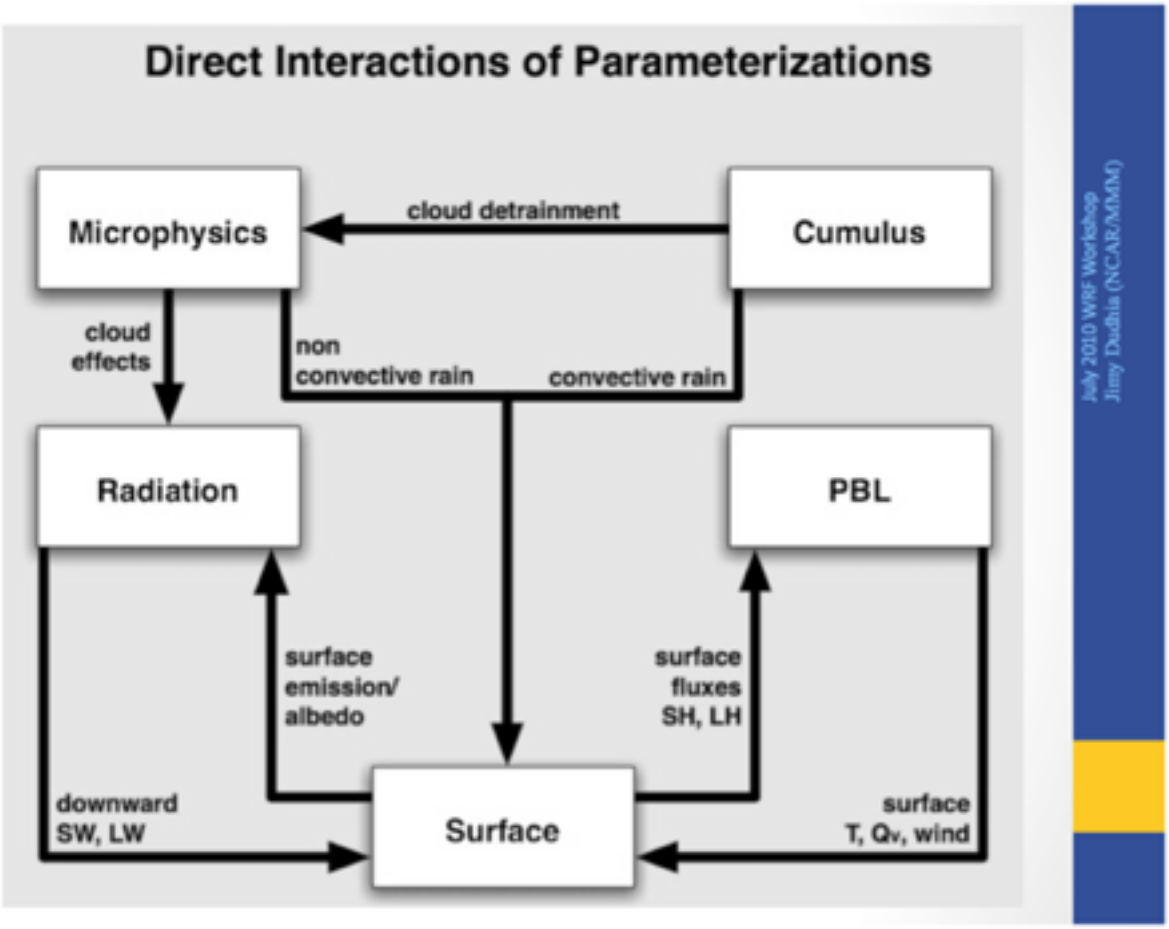

Figure 7: Figure is from a presentation by Jimy Dudhia at the WRF workshop in July 2010.

Kessler (1969) pioneered the introduction of the effect of varying updraughts into cloud models. In his approach, all water is first condensed as cloud water, with small drop size (roughly 5-30 micrometer) and negligible terminal velocity. Then a process called auto conversion begins. This involves the formation of precipitation particles either by the aggregation of several cloud particles or by the action of giant salt nuclei, or similar processes. Water clouds can persist for a long time without precipitating and various measurement show that cloud water contents of about 1 gm-3 are usually associated with precipitation (Mason, 1957; Singleton and Smith, 1960).

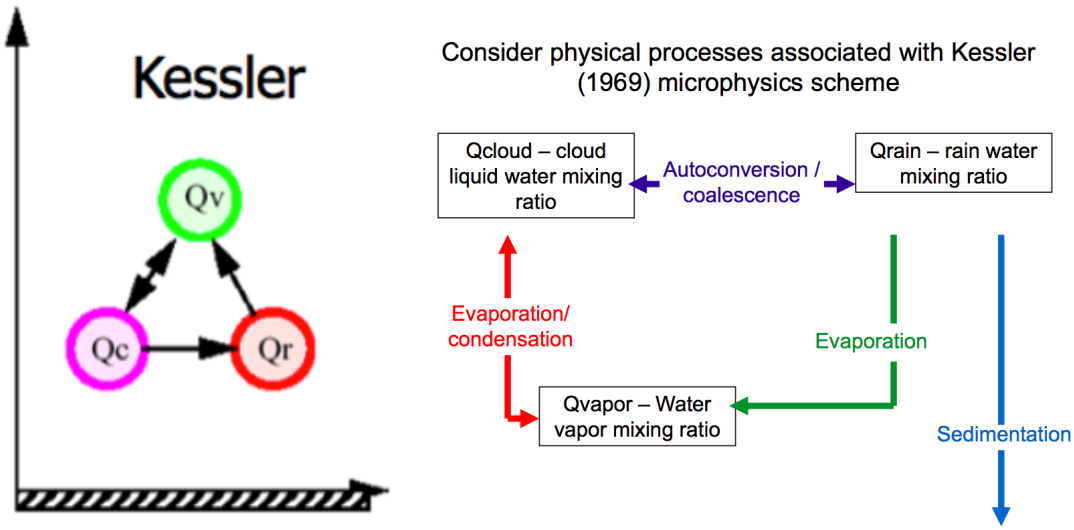

Figure 8: Flowchart of parameterization processes in Kessler scheme (NCAR presentation).

A bulk parameterization of cloud particles and precipitation drops based on the works of Lin et al. (1983) and Rutledge and Hobbs (1983) has been a primary option in representing cloud and precipitation processes in both General Circulation Models and mesoscale models. Hong et al. (2003) has suggested a revised approach to ice-microphysical processes in order to overcome the deficiencies identified by previous studies. Several modifications have been introduced to more realistically simulate some of the ice-microphysical processes. In addition to the assumption that ice nuclei number concentration is a function of temperature, a new and separate assumption is developed in which ice crystal number concentration is a function of ice amount. Related changes in ice microphysics are introduced, and the impact of sedimentation of ice crystals is also included. The revised ice-microphysics into WRF model improve model performance and this new approach is called WRF-Single- Moment-Microphysics scheme (WSMMPs). Together with the sedimentation of cloud ice, the new microphysics reveals a significant improvement in high-cloud amount, surface precipitation, and large-scale mean temperature through a better representation of

the ice- cloud/radiation feedback. WSM6 is one of the options for microphysics in WRF, since 2004. WSM6 scheme includes separate prognostic equations for water vapor, cloud water, cloud ice, snow, rain and graupel.

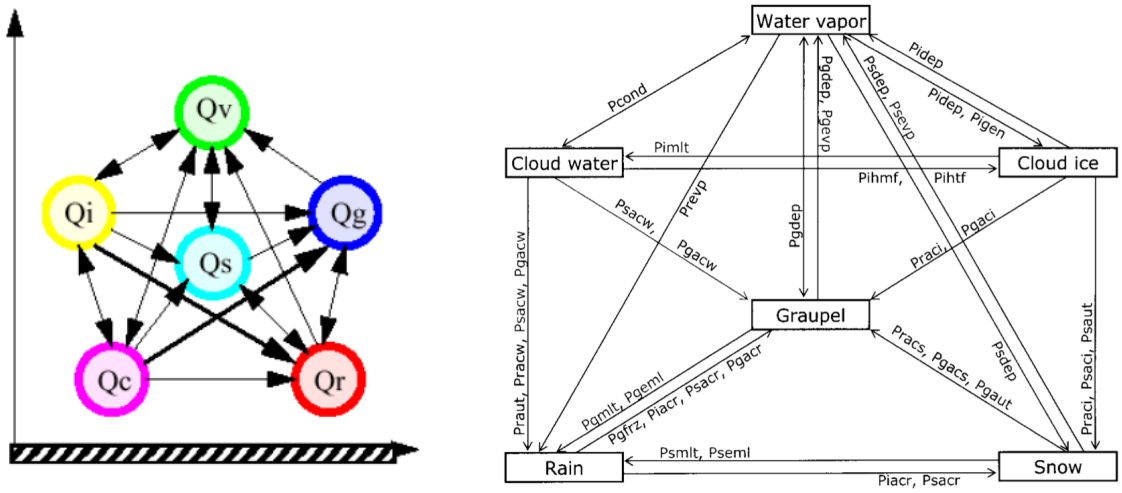

Figure 9: Flowchart of parameterization processes in WSM6 scheme (Hong and Lin 2006).

3.2.3 Other Parameterization Schemes

All other parameterization schemes were kept similar for MP1 and MP2 so the effect of microphysics could be evident. The Yonsei University (YSU) planetary boundary layer scheme [Noh et al., 2003; Hong et al., 2006] was used for surface fluxes and turbulent mixing in the boundary layer. RRTM-G schemes for both shortwave and longwave radiation [Iacono et al., 2008] were used. The Kain-Fritsch convective parameterization [Kain and Fritsch, 1990; Kain, 2004] was used in both the models. All the model selection given below in a tabular format. So the basic difference in model simulations is due to microphysics and based on that there could be four combinations which are as follows.

3.3 Description of Model Simulations

Based on two microphysics and two different stages of a tropical cyclone (Developing and Intensifying), each storm here (discussed in section xx) has four WRF simulations. Three storms will create a total of 12 scenario which will be analyzed. All these individual types are discussed belw in a tabular format.

Table 1. Classification based on model microphysics and stages of TCs.

Microphysics	**Developing Phase 'A'**	**Intensification Phase 'B'**
WSM6 (MP1)	**MP1A**	**MP1B**
Kessler (MP2)	**MP2A**	**MP2B**

Table 2. Description of phase 'A' and phase 'B' for each TC

STORM	**PHASE 'A'**	**PHASE 'B'**
CINDY	**0000UTC 17th Jun -0000UTC 19th Jun**	**0000UTC 19th Jun - 0600UTC 21st Jun**
MICHAEL	**1200UTC 6th Oct - 1200UTC 8th Oct**	**1800UTC 8th Oct – 1800 UTC 10th Oct**
IRMA	**0000UTC 30th Aug - 0000UTC 1st Sep**	**0000UTC 4th Sep – 0000 UTC 6th Sep**

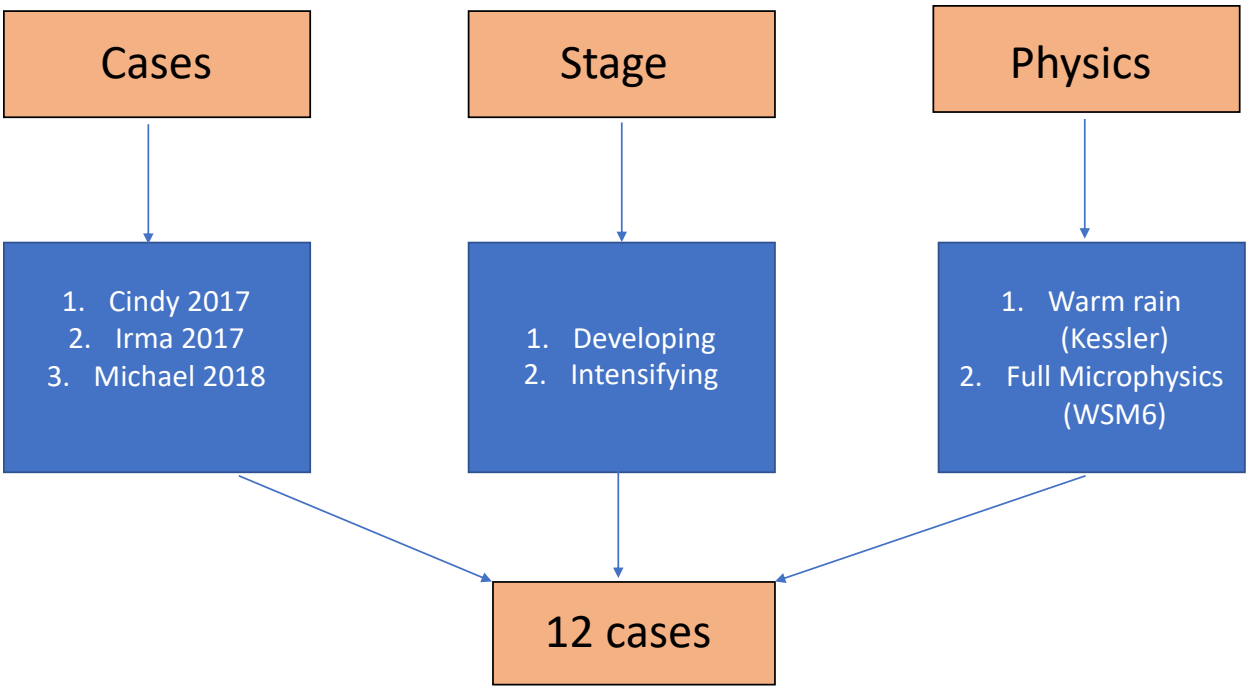

Figure 10. Schematic representation of different WRF simulations.

SELECTION OF DOMAIN FOR COMPUTATION

Using the first law of thermodynamics, the mass continuity equation and the time tendency of the vorticity, and divergence equations written in terms of the streamfunction (ψ) and velocity potential (χ), respectively, for a closed domain, one can easily arrive at the following set of equations following Krishnamurti and Ramanathan (1982):

$$\frac{\partial \overline{\overline{K}}_{\psi}}{\partial t} = \underbrace{\overline{\overline{f\nabla\psi.\nabla\chi}}}_{Term\ 1} + \underbrace{\overline{\overline{\nabla^2\psi\nabla\psi.\nabla\chi}}}_{Term\ 2} + \underbrace{\overline{\overline{\nabla^2\chi\left(\frac{\nabla\psi}{2}\right)^2}}}_{Term\ 3} + \underbrace{\overline{\overline{\omega J\left(\psi,\frac{\partial\psi}{\partial p}\right)}}}_{Term\ 4} + \overline{\overline{F}}_{\psi} + B_{\psi}$$

$$\frac{\partial \overline{\overline{K}}_{\chi}}{\partial t} = -\underbrace{\overline{\overline{f\nabla\psi.\nabla\chi}}}_{Term\ 1} - \underbrace{\overline{\overline{\nabla^2\psi\nabla\psi.\nabla\chi}}}_{Term\ 2} - \underbrace{\overline{\overline{\nabla^2\chi\left(\frac{\nabla\psi}{2}\right)^2}}}_{Term\ 3} - \underbrace{\overline{\overline{\omega J\left(\psi,\frac{\partial\psi}{\partial p}\right)}}}_{Term\ 4} - \underbrace{\overline{\overline{\chi\nabla^2\phi}}}_{Term\ 5} + \overline{\overline{F}}_{\chi} + B_{\chi}$$

Where, $J, K_{\psi}, K_{\chi}, \phi, B_y$ are Jacobian operator, kinetic energy of irrotational and non-divergent component of the winds, geopotential, and corresponding boundary flux terms, respectively. The overbars in Equations (x) and (x) represent domain average. In order to interpret the terms on the

right-hand side of Equations (32) and (33) it should be recognized that $\nabla^2\psi = \xi \; and \; \nabla^2\chi = D$ where, ξ and D are vorticity and divergence, respectively. Furthermore, $K_\chi = \frac{1}{2}[\nabla\chi]^2 \; and \; K_\psi = \frac{1}{2}[\nabla\chi]^2$. Since we are analyzing the terms in Equations 32 and 33 in the case of TCs, the domain average is represented at 850hPa by the radius from the center of the TC to the point at which the tangential wind varies asymptotically with the radius (example of Irma intensifying stage with WSM6 Fig. 11a). Similarly, at the outflow level, we mark the domain from the center of the TC to when the radial wind varies asymptotically with the radius (example of Irma intensifying stage with WSM6 Fig. 11b). It may be noted that the outflow level is designated based on the peak in the radial wind profile. These choices of the domain boundaries are deliberate to highlight the changes in the transformation of the kinetic energies in a TC as it will become clear when the results are discussed. Furthermore, the boundary flux terms are kept small by the choice of this domain. It is important to however note that these domain choices are not arbitrary and are objectively determined for each TC at a given time of its evolution.

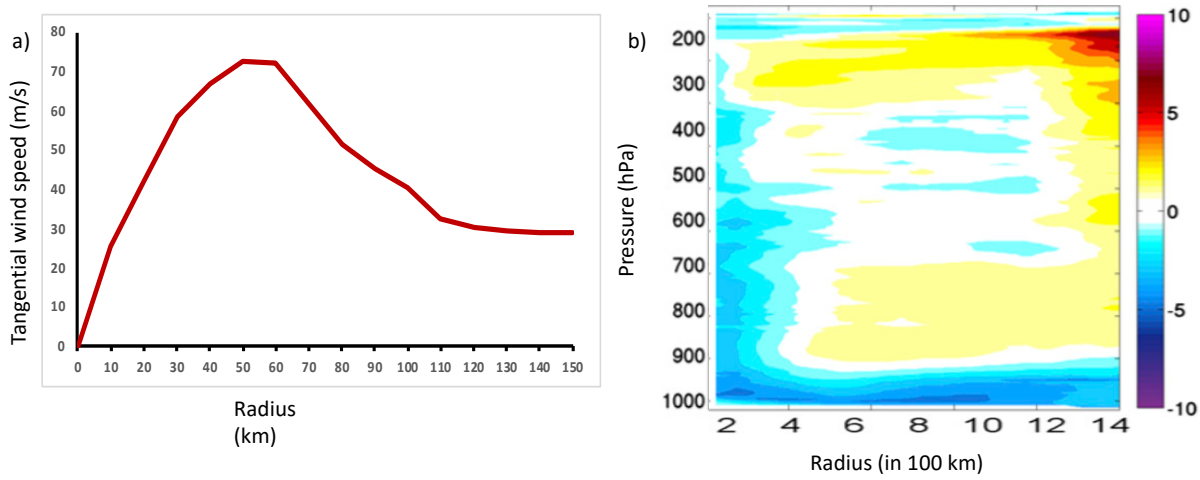

Figure 11. For TC Irma (2017) intensifying stage simulated with WSM6, a) Radial profile of tangential wind at 850hPa b) vertical profile of radial wind at outflow level (200hPa).

Table 3. Radius used to compute domain average for all TCs at developing and intensifying stages. 850hPa and outflow levels are represented separately for each stage and each TC.

850hPa for Developing Stage						
TC	Cindy		Michael		Irma	
Microphysics	WSM6	Kessler	WSM6	Kessler	WSM6	Kessler
Radius (km)	350	310	250	270	180	200
Outflow Level for Developing Stage						
TC	Cindy		Michael		Irma	
Microphysics	WSM6	Kessler	WSM6	Kessler	WSM6	Kessler
Radius (km)	450	400	850	790	1100	1050
Level (hPa)	400	400	350	350	250	250
850hPa for Intensifying Stage						
TC	Cindy		Michael		Irma	
Microphysics	WSM6	Kessler	WSM6	Kessler	WSM6	Kessler
Radius (km)	450	520	180	200	140	155
Outflow Level for Intensifying Stage						
TC	Cindy		Michael		Irma	
Microphysics	WSM6	Kessler	WSM6	Kessler	WSM6	Kessler
Radius (km)	950	800	1100	1000	1350	1250
Level (hPa)	350	350	250	250	200	200

CHAPTER 4

RESULTS AND DISCUSSION

All the tropical cyclones in this study have been simulated using the WRF model (version 3.8.1 with two microphysics WSM6 (experiment name: MP1) and Kessler (experiment name: MP2). The simulation period is divided into parts which has been explained in the previous section. To verify these model simulations, the simulated rain rates (mm/hr) are compared to the corresponding observed TRMM/GPM rainfall rates at every 6hr time interval over the model integration period. As a result of the differences in the two versions (MP1 and MP2) models, the simulations diverged from each other in both (incipient and mature) stages of tropical cyclones . The Kessler scheme which parameterizes only the warm rain process compared to WSM6 (which also includes the cold rain processes), produces copious amount of precipitation across the domain and the rain rates are also comparatively higher than WSM6. Whereas, WSM6 experiments (MP1A and MP1B) produce comparable precipitation relative to the observations both in terms of their spatial structure and intensity. Zhu et al. (2006) also found in their study that the Kessler microphysics scheme had a tendency to produce higher rain rates, a weaker tropical cyclone with a wider area of precipitation and more cloud coverage in the eyewall as observed in the Kessler simulations of this study.

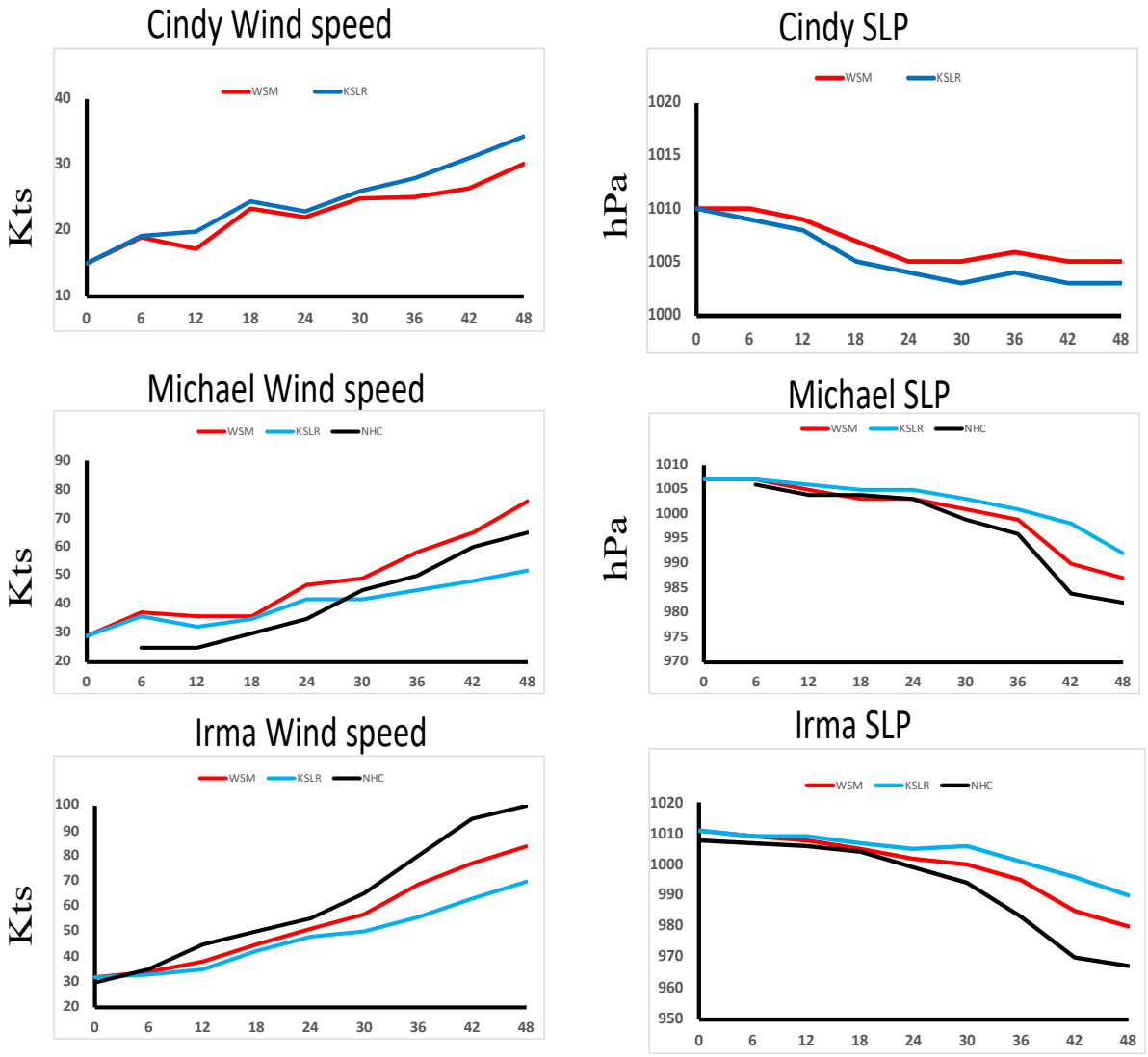

Figure 12. Comparison of simulated maximum sustained wind speed and minimum sea level pressure between WSM6 (MP1in Red) Kessler (MP2 in Blue) and NHC observed (black)during phase 'A' i.e. developing stage.

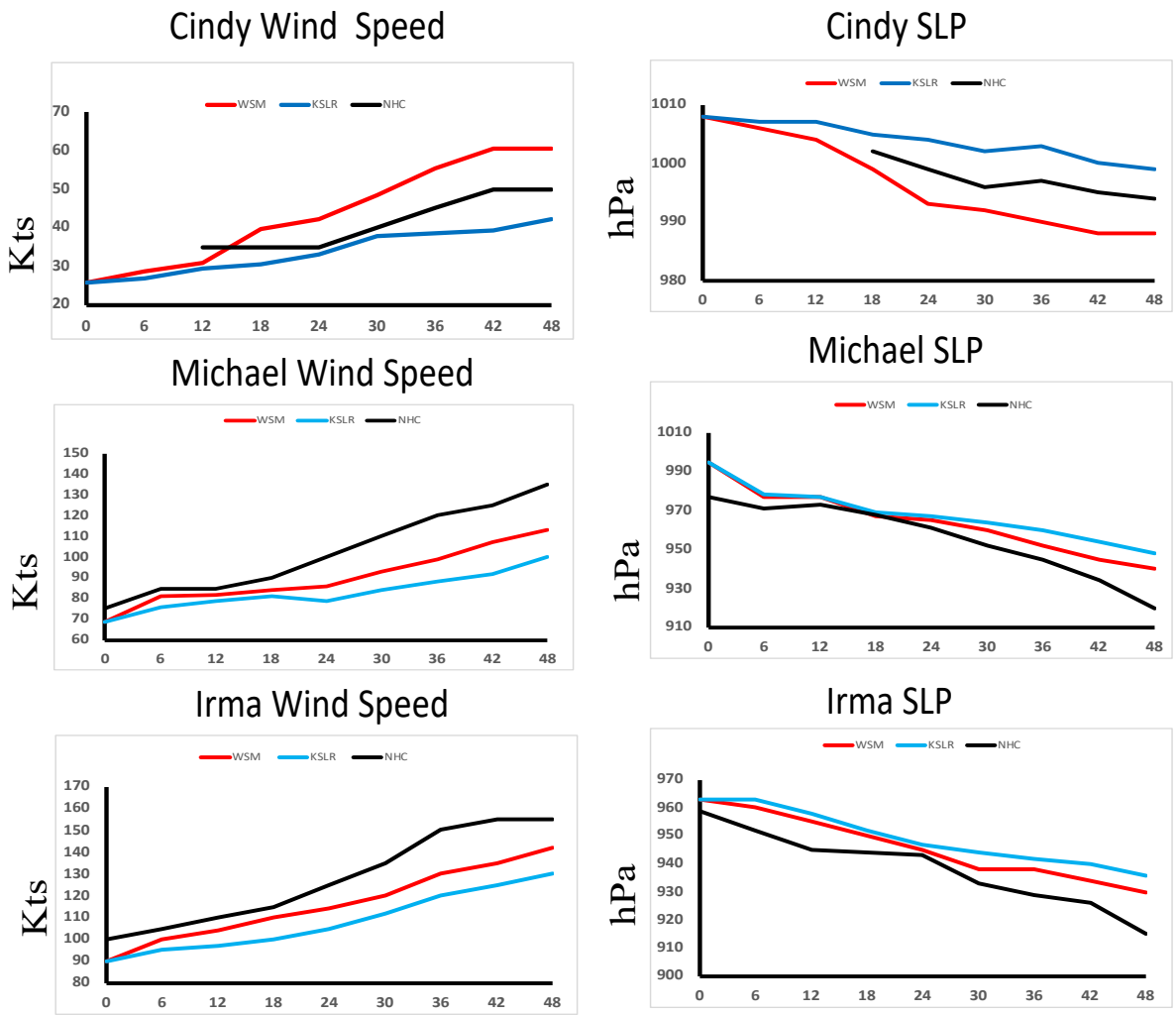

Figure 13. Comparison of simulated maximum sustained wind speed and minimum sea level pressure between WSM6 (MP1in Red) Kessler (MP2 in Blue) and NHC observed (black)during phase 'B' i.e. intensifying stage.

Over the period of the model simulations, the maximum sustained wind speed (Vmax; at 10m above the surface) and point of minimum sea level pressure have been determined at intervals of 6 hours. The verification of the model simulations in terms of the time evolution of the maximum sustained wind speed and minimum SLP is shown in Fig. 12 and Fig. 13. It should be mentioned that since TC Cindy did not attain tropical storm status till 1800 UTC of the 19th June, the

verification data from HURDAT is unavailable in the initial period of its simulation. We note that the model simulation overestimates the wind speed and minimum SLP in the case of TC Cindy, throughout its evolution (Fig. 13). In the remaining two cases (Michael and Irma), the model simulation underestimates the maximum wind speed and minimum SLP, which is in contrast to the simulation of Cindy (Fig. 12 and Fig.13). It may be noted that another exception occurs in the case of Cindy where Vmax is higher in MP2 relative to MP1 by the end of the genesis period i.e. 19th June 0000UTC. But MP1B produces stronger Vmax than MP2B in the mature stage (20th June 1800 UTC) when the disturbance was declared tropical storm Cindy by NHC. With such conflicting results, it is hard to understand the superiority of one microphysics scheme over the other. It is our contention that the analysis of psi-chi interactions is likely to reveal the underlying reasons for such conflicting results.

Comparison of max. sustained wind speed and min. sea level pressure shows that there is significant differences in the simulations of these tropical cyclones between the adoption of the two microphysics schemes. The rain rate values associated with Kessler is higher throughout the simulation periods in both the phases relative to WSM6. However, the max. sustained wind speed is always higher (or min sea level pressure lower) in MP1 than MP2. This difference in modeled intensity could be due to the difference in their vertical distribution of the diabatic heating generated by each of the microphysical schemes. Previous studies suggest that the simulated intensity can be influenced by the choice of the microphysics schemes. The simulations with WSM6 scheme are found to have lower MSLP than that with the Kessler scheme and similarly, WSM6 achieves a higher maximum wind speed than the Kessler scheme. The choice of the microphysics influence the intensity and amount of precipitation of a tropical cyclone by controlling the generation of diabatic heating. Chan and Chan (2016) show that WSM6 compared

to Kessler scheme produces more diabatic heating and that generates higher upper-tropospheric divergence and lower-tropospheric convergence, which in turn results in a simulation with higher TC intensity with the WSM6 scheme. This result is consistent with the reported differences in the intensity between MP1 and MP2 in phase B. However, this argument fails in phase A of the development of tropical storm Cindy.

The main purpose of this study is to understand the role of psi-chi interaction over the evolution of the tropical cyclone. To achieve this objective, a domain averaged kinetic energy associated with the irrotational component of wind and the non-divergent component (following Eqn. 32) of the wind have been computed and plotted for MP1A, MP1B, MP2A and MP2B at 850hPa and outflow level.

The individual terms of psi-chi energy interaction equations are computed. It is found that domain average value of Term 1 and Term 2 (of Eqn. 32) are the major contributors. Terms 1 and 2 are in the order of 10^{-4} at intensifying stage. Term 3 and Term 4 are one and two orders of magnitude smaller than 10^{-4} and 10^{-5} respectively. So, henceforth the firs three terms (Terms 1, 2 and 3) have been considered. The evolution for all three terms show variation in genesis (phase A) and intensification (phase B) stages of each of the tropical cyclones examined in this study. As the tropical cyclone grows and strengthens, the vorticity of the cyclonic circulation increases which contributes to the Term 2. In this case, tropical cyclones Cindy and Michael, they move from the Caribbean region to the more northward location of the GoM and on the other hand Irma moved northward in Atlantic. Therefore, the Coriolis force represented by 'f' will change positively as the cyclones move northward, which leads to the growth of Term 1. In other words, the increase in vorticity and Coriolis force will contribute to the growth of Terms 1, 2 and 3 and eventually towards the 'total' term with time i.e. from phase A to phase B of the tropical cyclone.

For each simulation the area of interest i.e. the region to be considered for domain average are calculated based on the radial profile of tangential wind at 850 hPa and vertical profile of radial wind used to determine the outflow layer and its boundary (based on Table 3). So for every storm this area will differ from other. Not only for storms but the area under consideration will also change for simulations of different microphysics schemes and stages of tropical cyclones. So the magnitude of kinetic energy terms and individual terms of equation 32 will vary from one simulation to other. To understand the results better they are represented in three categories : a) Understanding $\psi - \chi$ framework for intensifying tropical cyclones, b) understanding the Sensitivity of the TC simulations to changes in microphysics and c) understanding the Sensitivity of the TC simulations to changes in stage of evolution

a) Understanding $\psi - \chi$ framework for intensifying tropical cyclones

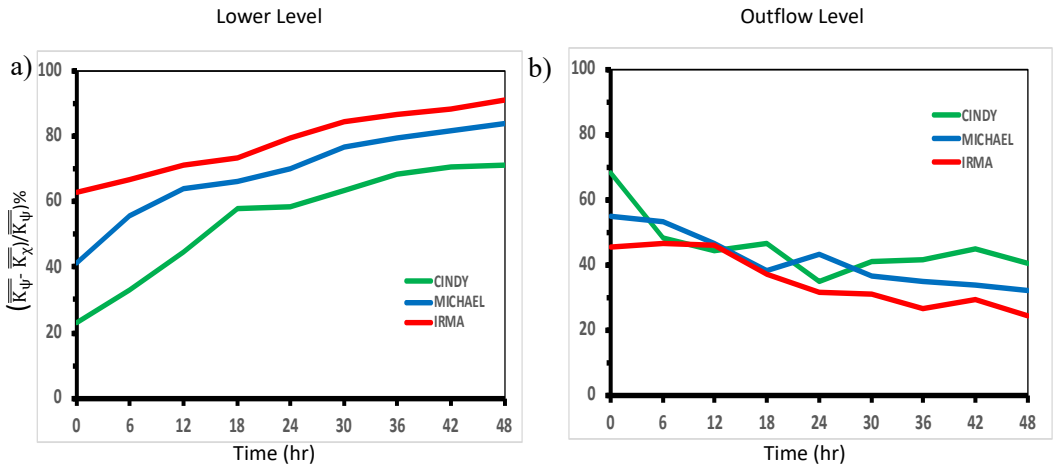

Figure 14. The time series of the fractional conversion of irrotational to non-divergent kinetic energy at a) 850hPa and at b) the outflow level from the WRF simulations of TCs Cindy 2017, Irma 2017, and Michael 2018.

In Fig. 14 we show the time series of the fractional conversion of $K_\chi \; to \; K_\psi$ ($\equiv C_{\chi\to\psi} = \left(\frac{K_\psi - K_\chi}{K_\psi}\right) \times 100$) at 850hPa for all three TCs computed from the corresponding WRF simulations. It is seen clearly from the figure that consistent with the evolution of the intensity of the TC, this fractional conversion is highest for Irma followed by that for Michael and then Cindy at 850hPa (Fig. 14 a). In addition, we also see from the figure that $C_{\chi\to\psi}$ at 850hPa evolves with the intensity of the TC. $C_{\chi\to\psi}$ is small at the beginning of the simulation and grows to its peak value towards the end of the simulation, when the TC attained its maximum intensity (Fig. 13). In contrast, the evolution of $C_{\chi\to\psi}$ in the outflow level in Fig. 13 shows its magnitude decreasing through the simulation in the case of Irma and Michael but not as much in the case of Cindy. TCs Irma and Michael were significantly more intense than Cindy and therefore the contrasting evolution of $C_{\chi\to\psi}$ at the outflow level in TC Cindy relative to the other two TCs (Fig. 14) is a reflection of their varied evolution. It may be noted that at their peak intensity, the outflow level (at which $C_{\chi\to\psi}$ in Fig. 14 b is shown) was diagnosed as 350hPa, 250hPa, and 200hPa for TCs Cindy, Michael, and Irma, respectively. It is suggested here that the relative reduction in $C_{\chi\to\psi}$ in the outflow level with time in Michael and Irma causes an increased likelihood for the intensification of the TC as it retains more kinetic energy for the irrotational component of the flow, and hence for the radial outflow. This follows from Rappin et al. (2009), who showed that the energy sink of the secondary circulation is minimized by the weak inertial stability in the outflow layer which leads to rapid intensification of the TC. They suggest that the preferred outflow channels in rapidly intensifying TCs form in regions of least resistance that are characterized by weak environmental inertial stability. In a similar vein, Merrill (1988) documented that in intensifying TCs the outflow is influenced by upper level synoptic features in contrast to non-intensifying TCs. Similarly, the

relative reduction of the growth in K_ψ in the outflow layer at the expense of K_χ leads to a favorable environment for the intensification of the TC.

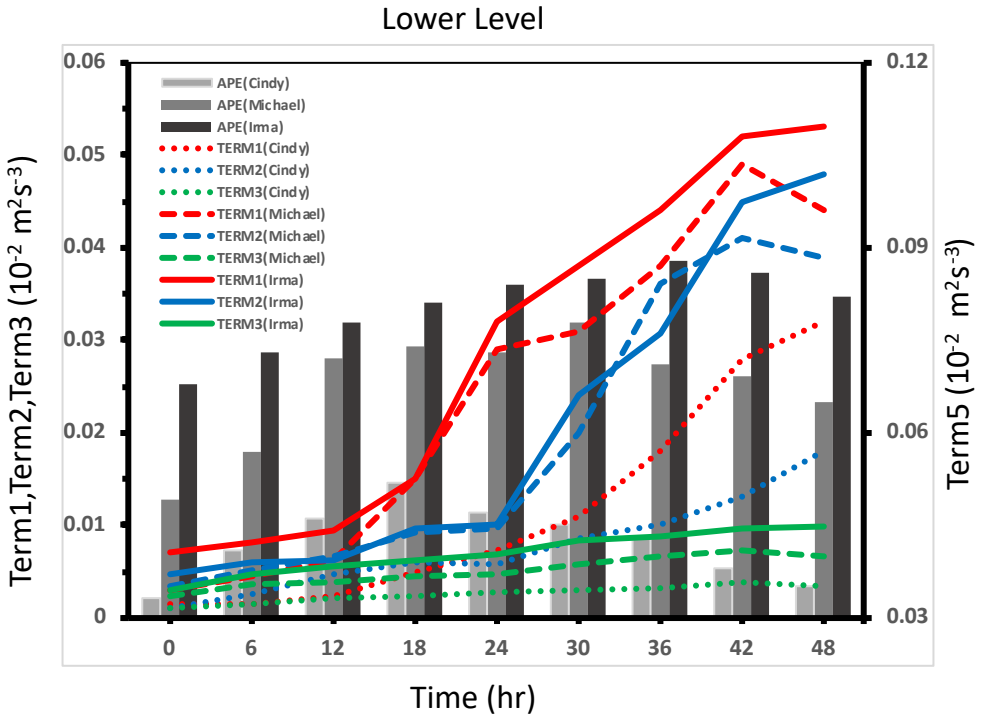

Figure 15: The transformation terms (Terms 1, 2, 3, of Equation 1(lines) and Term 5 (column) of Equation 32 in text) for TC at 850hPa of TCs Cindy 2017, Irma 2017, and Michael 2018.

In Fig. 15 we show the time series of the first three terms of Equations 1 and 2 and Term 5 of Equation 2 for all three TCs at 850hPa, which indicate that Term 1 is dominant followed by Term 2, and then Term 3. The generated APE is proportionately higher in the stronger TCs (Michael and Irma) relative to the weaker TC (Cindy). The comparative magnitudes of all these terms between the three TC cases is also reflective of their relative differences in intensity (Fig. 13).

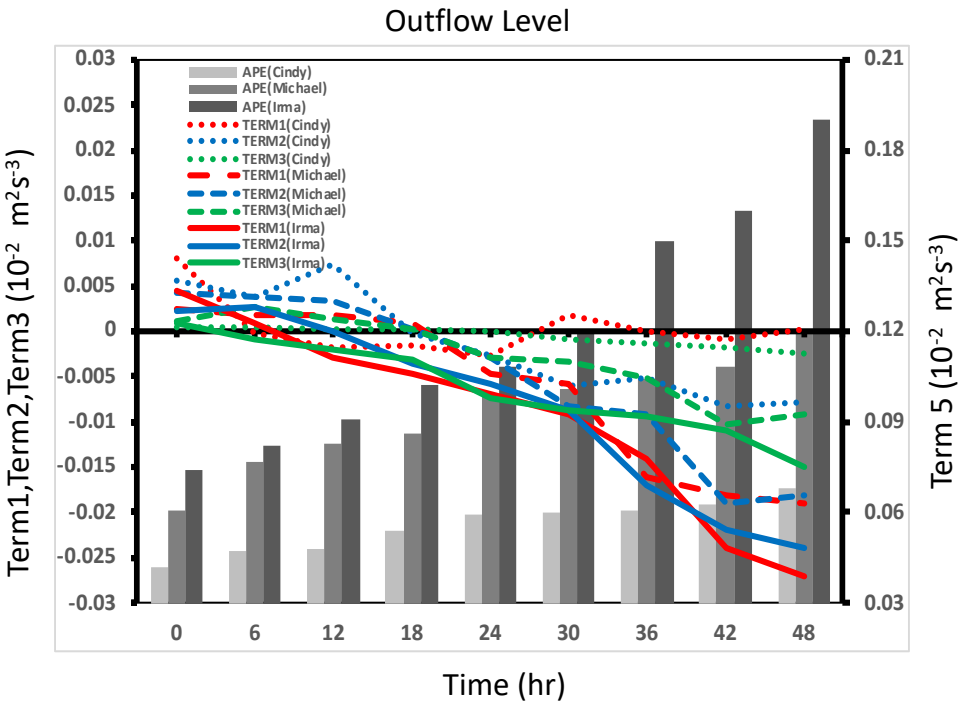

Figure 16: The transformation terms (Terms 1, 2, 3, of Equation 1 (lines) and Term 5 (columns) of Equation 2 in text) in the outflow layer for TC a) Cindy 2017, b) Irma 2017, and c) Michael 2018.

In the outflow level (Fig. 16) these three forcing terms of Equation 32 have opposite sign relative to those at 850hPa (Fig. 15). At the initial time of the evolution of TCs Michael and Irma, these terms are marginally positive and then eventually they grow to large negative values towards the end of the simulations. These negative values suggest they are a sink to K_ψ and a source for K_χ at the outflow level within the domain wherein the radial velocity is relatively large. Again, the relative magnitude of these terms in Fig. 16 suggest that the larger negative values serve to intensify the TC while smaller negative values tend to weaken the TC. It is interesting to note that APE at this outflow level is higher than at 850hPa (Fig. 15) for all three TCs and yet the conversion of K_χ to K_ψ is far less than at 850hPa. This is because the orientation of the gradients of ψ and χ

are not conducive for this conversion (Fig. 18). Unlike at 850hPa (Figs 17), here the gradients of ψ and χ across the three TCs at their peak intensity is far more comparable (Figs. 12).

The magnitude of $'(|\nabla\psi||\nabla\chi|cos\theta)'$ is not only dictated by the magnitude of the gradients of ψ and χ but also by the angle (θ) between the gradients. In Figs. 17 a-c we show the product of the gradients of ψ and χ as a function of θ at the time of peak intensity of all three TCs. Systematically we see in Figs. 17 that the dot products of the gradients of ψ and χ is lowest in the weakest TC (Cindy) and highest in the strongest TC (Irma), a reflection of relative differences in the magnitudes of their gradients. We also consistently observe in Figs. 16 that there is a greater density of points with gradients of ψ and χ to be aligned with negative values of cosθ (i.e., the angles [θ] are between 90° and 180°) for weaker storms (e.g. Cindy; Fig. 16) relative to the stronger storms (e.g Michael and Irma; Figs. 17; See also Table 4). Likewise, between Michael (Fig. 16) and Irma (Fig. 17), one observes that Michael displays a larger density of points with angles between 90° and 180° than Irma at their peak intensity (Table 4). In other words, gradients of ψ and χ at 850hPa in the large-scale TC environment are relatively less parallel in Michael than in Irma. As Fig. 18 shows in comparison to Fig. 17, a majority of the points in the environment of these TCs through their evolution have an angle between 90° and 180° (Table 4), which renders their dot product to be overall negative. In Fig. 18 we observe that the density of points with the gradients of ψ and χ having an angle between 90° and 180° is lower for weaker TCs like Cindy than stronger TCs like Michael and Irma (Table 4). In addition, between Michael and Irma, it is apparent that the density of points with angles between 90° and 180° is higher for the latter than the former (Figs. 18 ; Table 4). Therefore, the conversion $C_{\chi\rightarrow\psi}$ at the outflow level of the stronger

TCs is less efficient than the weaker TCs thereby reducing the inertial stability and the resistance of the outflow.

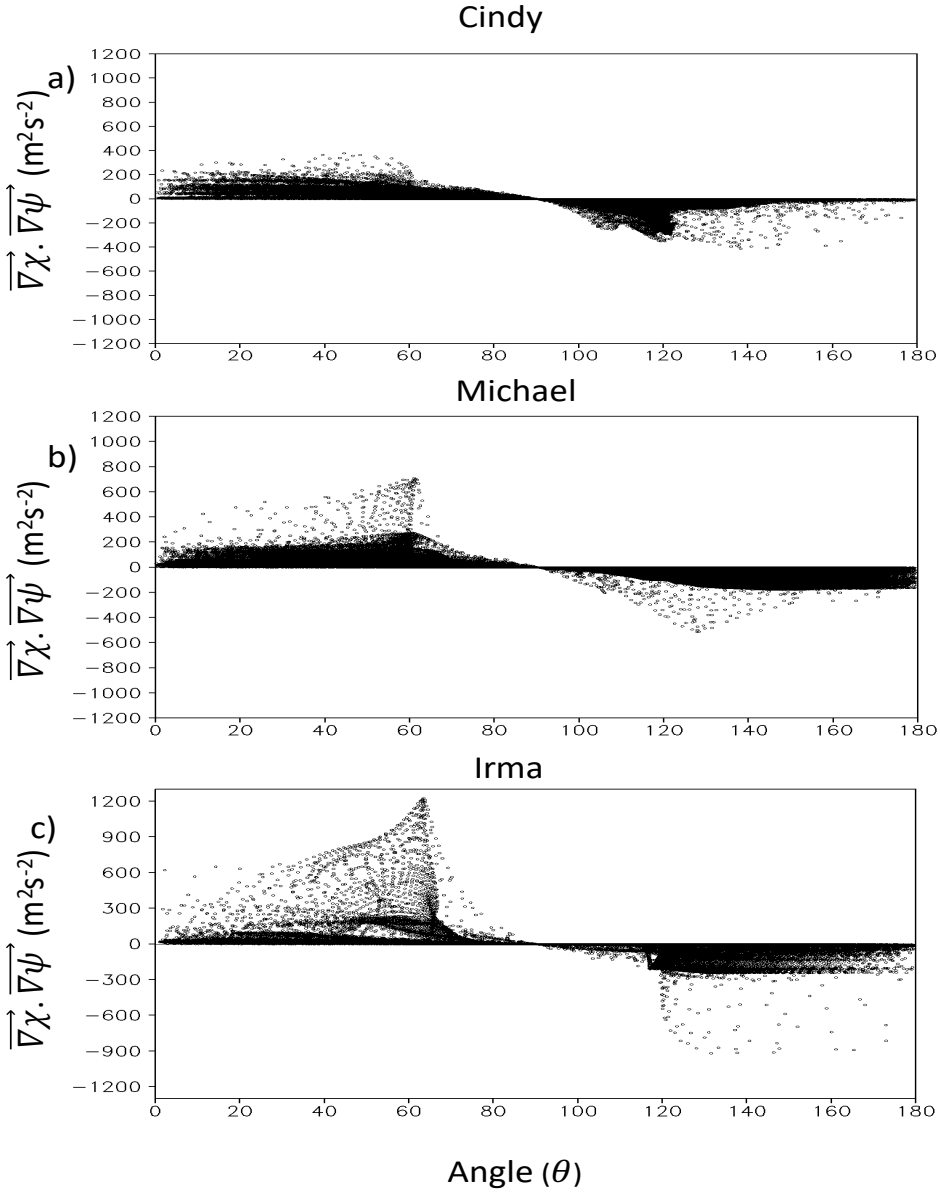

Figure 17. $(\nabla\psi.\nabla\chi)$ as a function of the angle (in degrees) between the gradients of ψ and χ at 850hPa of TCs (a) Cindy 2017, (b) Michael 2018 and c) Irma 2017 when they reach their peak intensity.

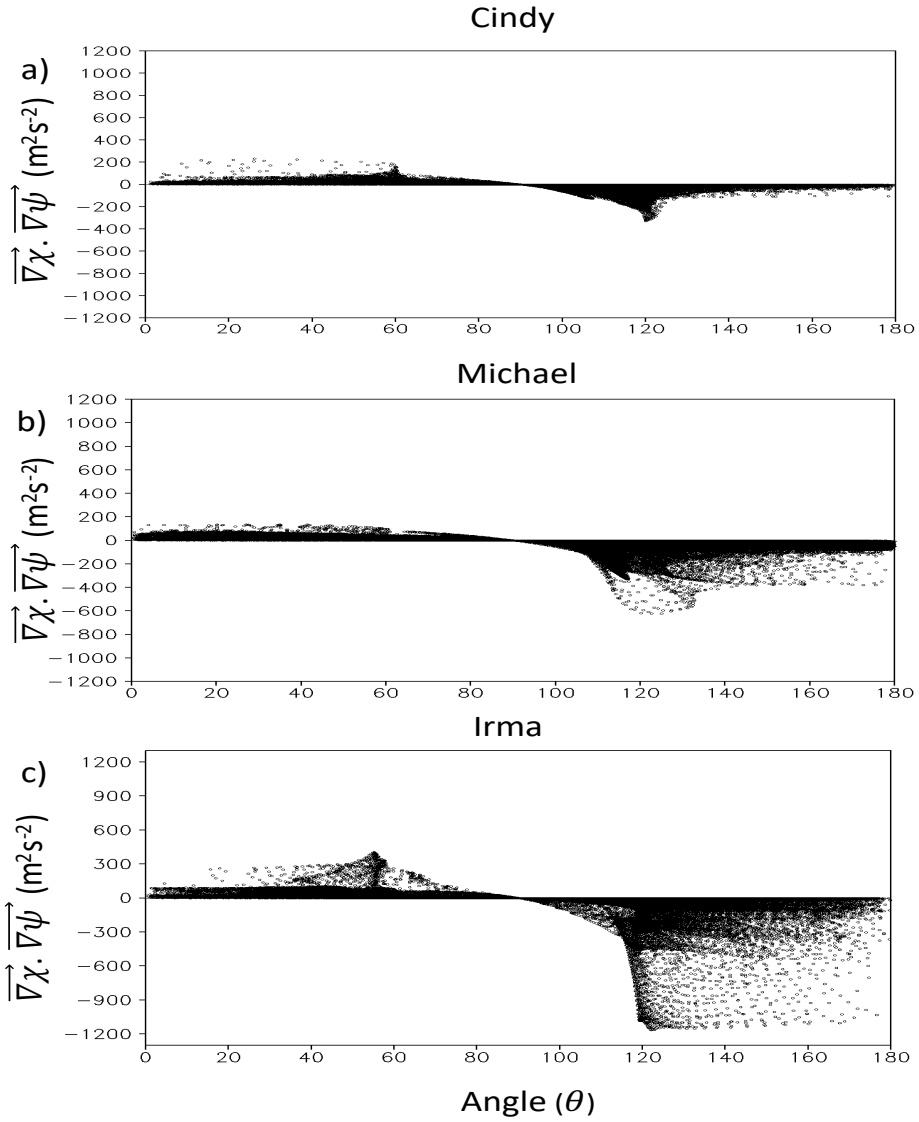

Figure 18. The dot product of the gradients of ψ and χ ($\nabla\psi.\ \nabla\chi$) as a function of the angle (in degrees) between the gradients of ψ and χ at the outflow level of TCs (a) Cindy 2017 at 350hPa, (b) Michael 2018 at 250hPa, and (c) Irma 2017 at 200hPa, when they reach their peak intensity.

Table 4: The tally of the points with positive and negative orientation of the gradients of ψ and χ in Figs. 17 and 18.

Figure 17 (at 850hPa)			
TC	Cindy	Michael	Irma
Angle < 90	28443	32428	37291
Angle > 90	25812	20071	17709
Figure 18 (at outflow level)			
TC	Cindy	Michael	Irma
Angle < 90	39818	30941	25407
Angle > 90	40244	48827	57775

b) Understanding the sensitivity of the TC simulations to changes in microphysics

In a similar manner as discussed for explaining the varying evolution of the three TC case studies, we examine here the sensitivity of the simulation of the three Atlantic Tropical Cyclones (TCs) to two different microphysics schemes with one scheme including the mixed phased clouds i.e. WSM6 (MP1) and the other which includes only the warm rain process i.e. Kessler (MP2). The results show that the simulations with the mixed phase clouds verify better and the TCs are more intense than the simulations with only the warm rain process included (Fig 11 and 12). We analyze these differences in terms of the transformation of the kinetic energy from the irrotational the nondivergent component of the wind.

In Fig. 14 we show the comparative time series of the fractional conversion of K_χ to K_ψ ($\equiv$ $C_{\chi\to\psi} = \left(\frac{K_\psi - K_\chi}{K_\psi}\right) \times 100$) both at 850hPa and outflow level for all three TCs with both microphysics schemes. As the storm gets stronger from Cindy to Michael to Irma K_ψ shows an increasing trend and K_χ a decreasing trend at 850hPa (Fig.19 a, b and c) implying efficient energy conversion. This basic trend is present both in MP1 and MP2 but they differ in magnitude. MP1

is always associated with higher values of K_ψ and lower values of K_χ compared to MP2, irrespective of the case studies at 850hPa. So in Kessler scheme the conversion of the irrotational kinetic energy is to corresponding nondivergent kinetic energy is less efficient than WSM6. At the outflow level (Figs.19 d, e and f) both the energy terms shows increasing trend but here Kessler (MP2) produces more nondivergent kinetic energy than WSM6 (MP1).

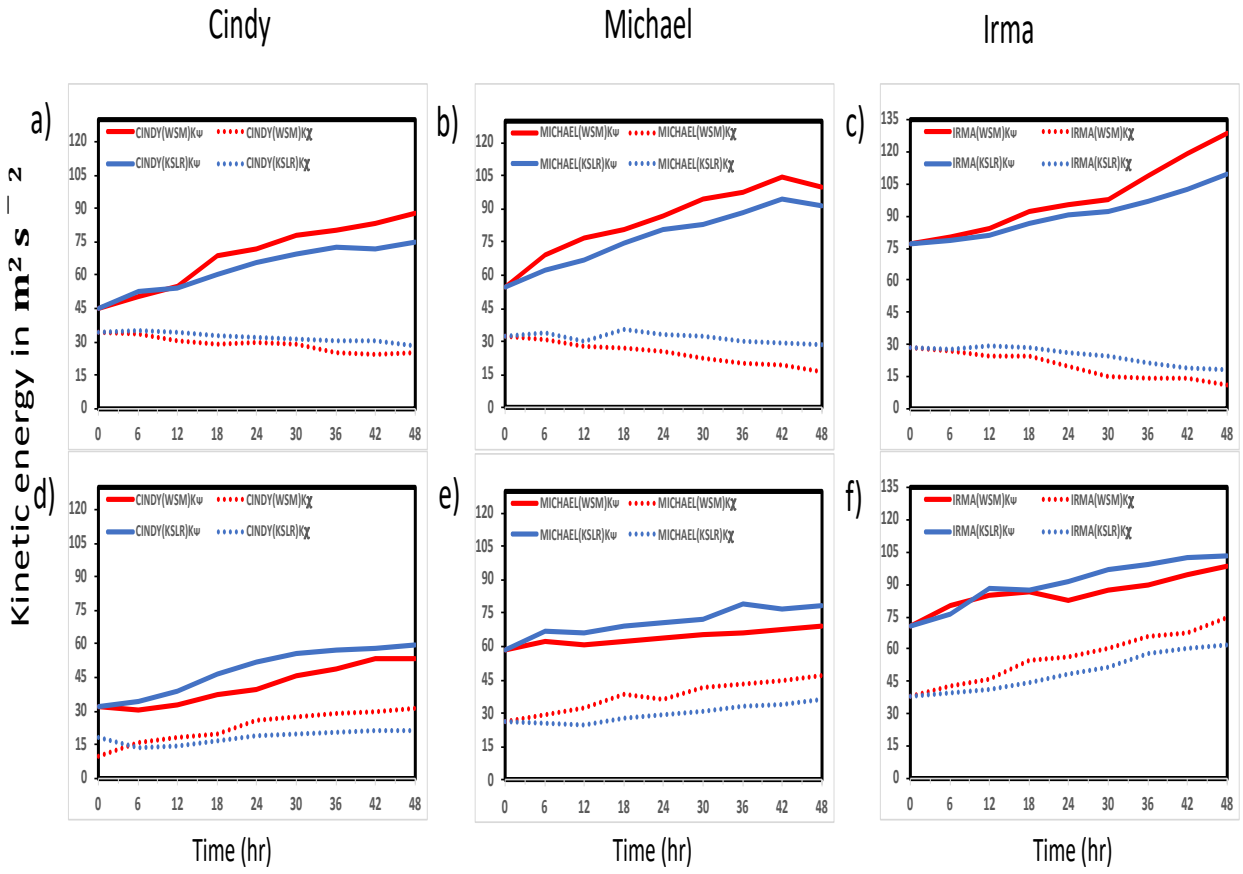

Figure 19. The time series of the irrotational (K_χ) and nondivergent (K_ψ) kinetic energy for (a, d) Cindy 2017, (b, e) Michael 2018, and (c, f) Irma 2017 for (a, b, c) 850hPa and (d, e, f) outflow simulations. The red and blue lines in each panel are for the WSM and Kessler schemes.

We find from this framework that the available potential energy (APE) in MP1 is less than in MP2 at 850hPa (Figs. 20 a, b, and c). It is because, there is more available energy transformed from the irrotational to the nondivergent component of the wind in MP1 relative to MP2, which is enabled by the first three terms of the transformation equation (Eqn 32). Examining these terms (Term1, Term2 and Term3 of Equation 32), which all show positive values (Fig.20 a, b, and c), it is evident that the rate of increase of these terms is higher in MP1 than in MP2. Now at outflow level (Fig. 20 d, e, and f), the trend of all these terms remain same as before (as in Fig. 16) irrespective of the choice of the microphysics scheme. It is seen in Fig. 20 d, e, and f that APE is lower in MP2 and that allows rate of change of irrotational to non-divergent kinetic energy higher in MP2 than MP1, for all three tropical cyclone cases, causing the diffluence of the outflow level to be stronger in MP1 (WSM6) than in MP2 (Kessler).

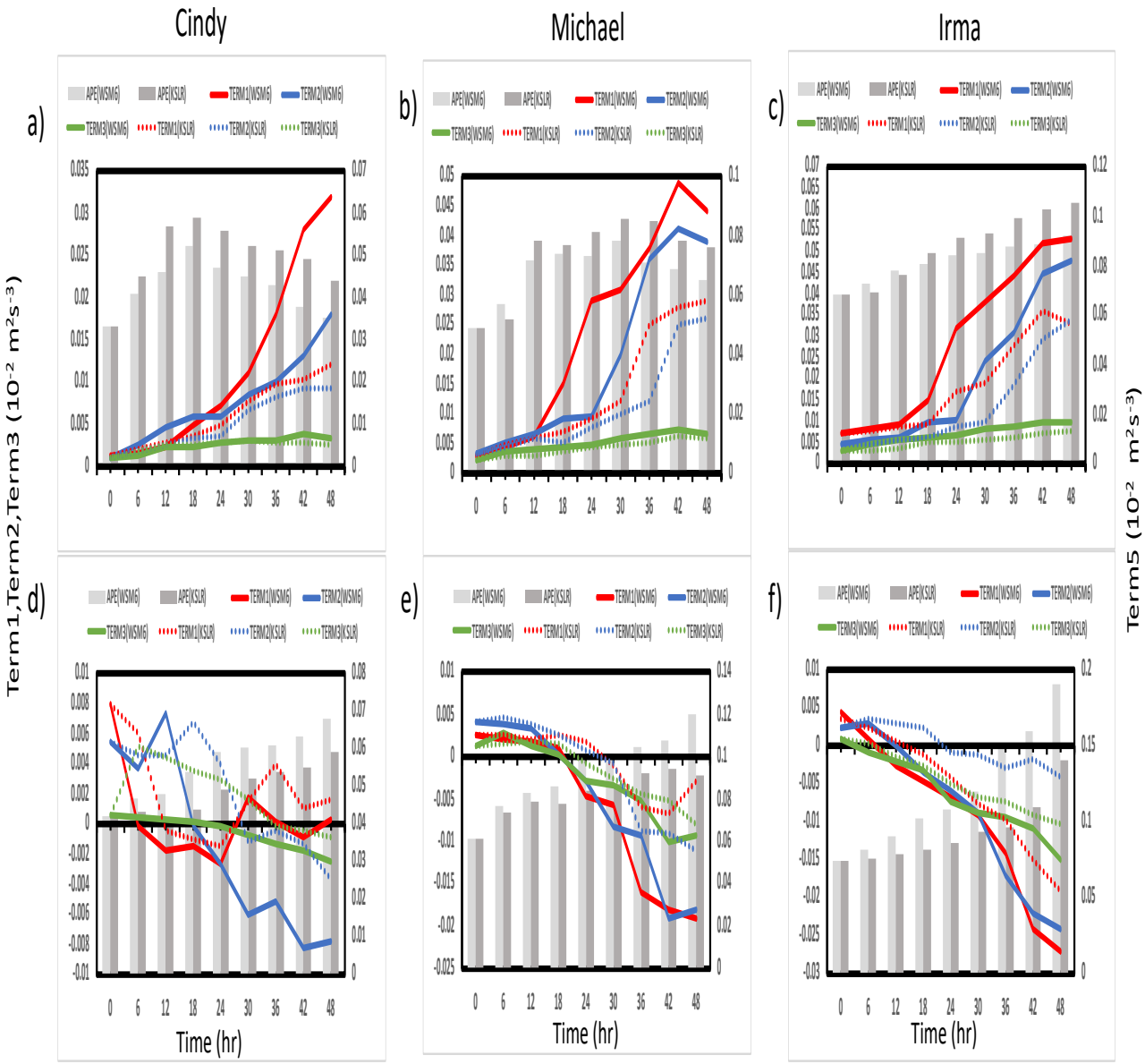

Figure 20. The transformation terms (Terms 1, 2, 3 of Equation 30 and Term 5 of Equation 32) at 850 hPa for TC (a, d) Cindy 2017, (b, e) Irma 2017, and (c, f) Michael 2018 for (a, b, c) 850hPa and (d, e, f) outflow level. Solid lines are for WSM6 and dotted lines are for Kessler scheme.

The difference in the values of the transformation terms (Terms 1 and 2) between MP1 and MP2 is primarily due to the difference in the dot product of the gradients of streamfunction and velocity potential. In general, the dot product grows higher as the storm gets stronger for both WSM6 (MP1) and Kessler (MP2). But the distribution of this transformation change not only with level (from inflow to outflow level) but also with changes in microphysics (Fig. 21 and Fig. 22). The general rule for different levels are discussed in previous Fig. 16 and 17, stands true here also. At 850hPa the number of points that lies between angle range (between the gradients of stream function and velocity potential) of 0^0-90^0 in MP1 is higher than in MP2 and points with angle range of 90^0-180^0 is lower in MP1 than in MP2, promoting as a result stronger circulation of the TC at lower level for MP1 i.e., WSM6. At the outflow level, there is a stark difference in the two microphysics schemes: MP1 shows more points that lies in the angle range 90^0-180^0 than MP2, whereas, the number of points that stay in the category of the angle range of 0^0-90^0 is higher in MP2 than MP1 (Table 5). The combination of these two makes the outflow layer more divergent in nature in MP1 than in MP2.

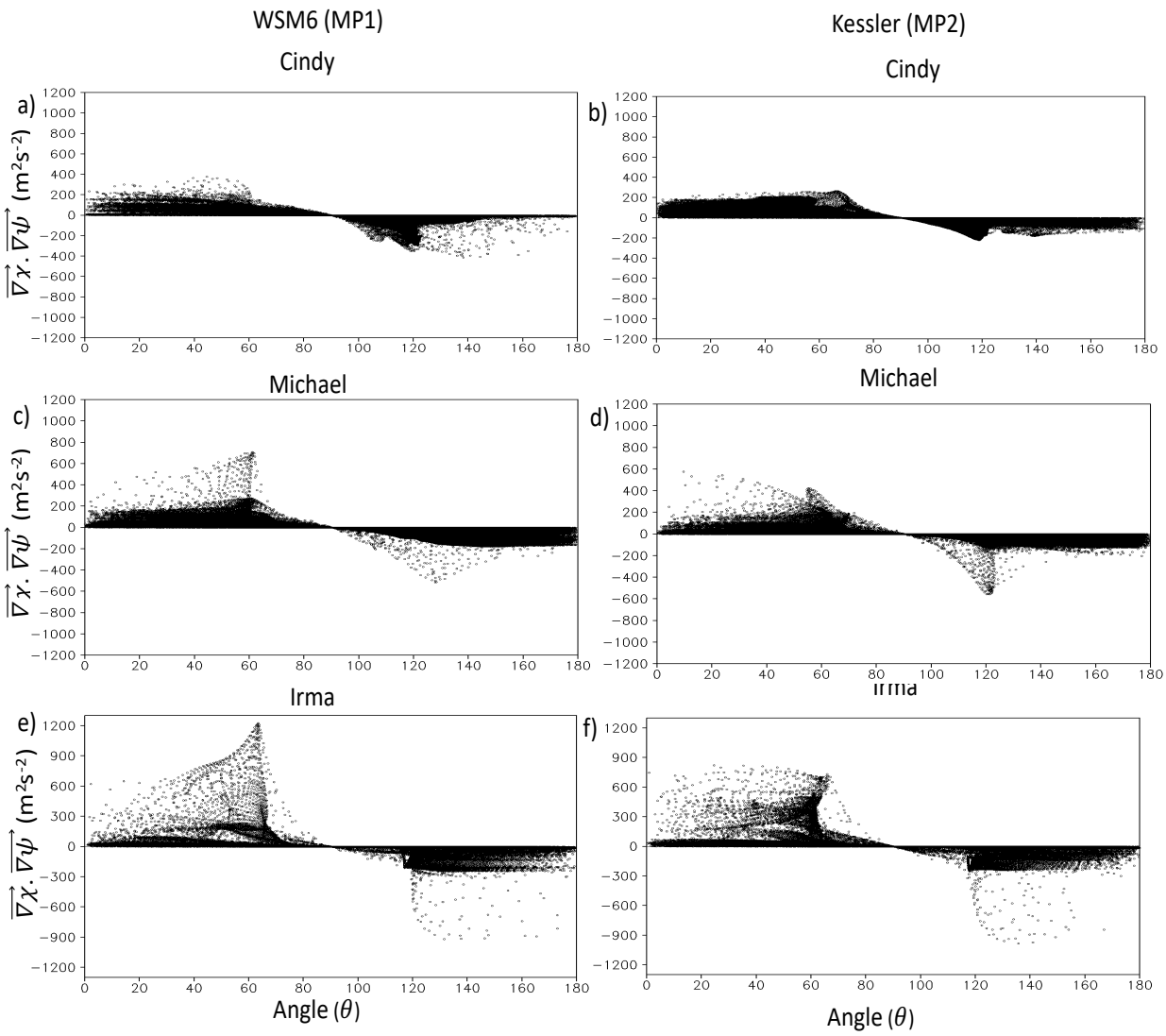

Figure 21. $(\nabla\psi.\nabla\chi)$ as a function of the angle (in degrees) between the gradients of ψ and χ at 850hPa of TCs (a, b) Cindy 2017, (c, d) Michael 2018 and (e, f) Irma 2017 when they reach their peak intensity. (a, c, e) for WSM6 and (b, d, f) for Kessler.

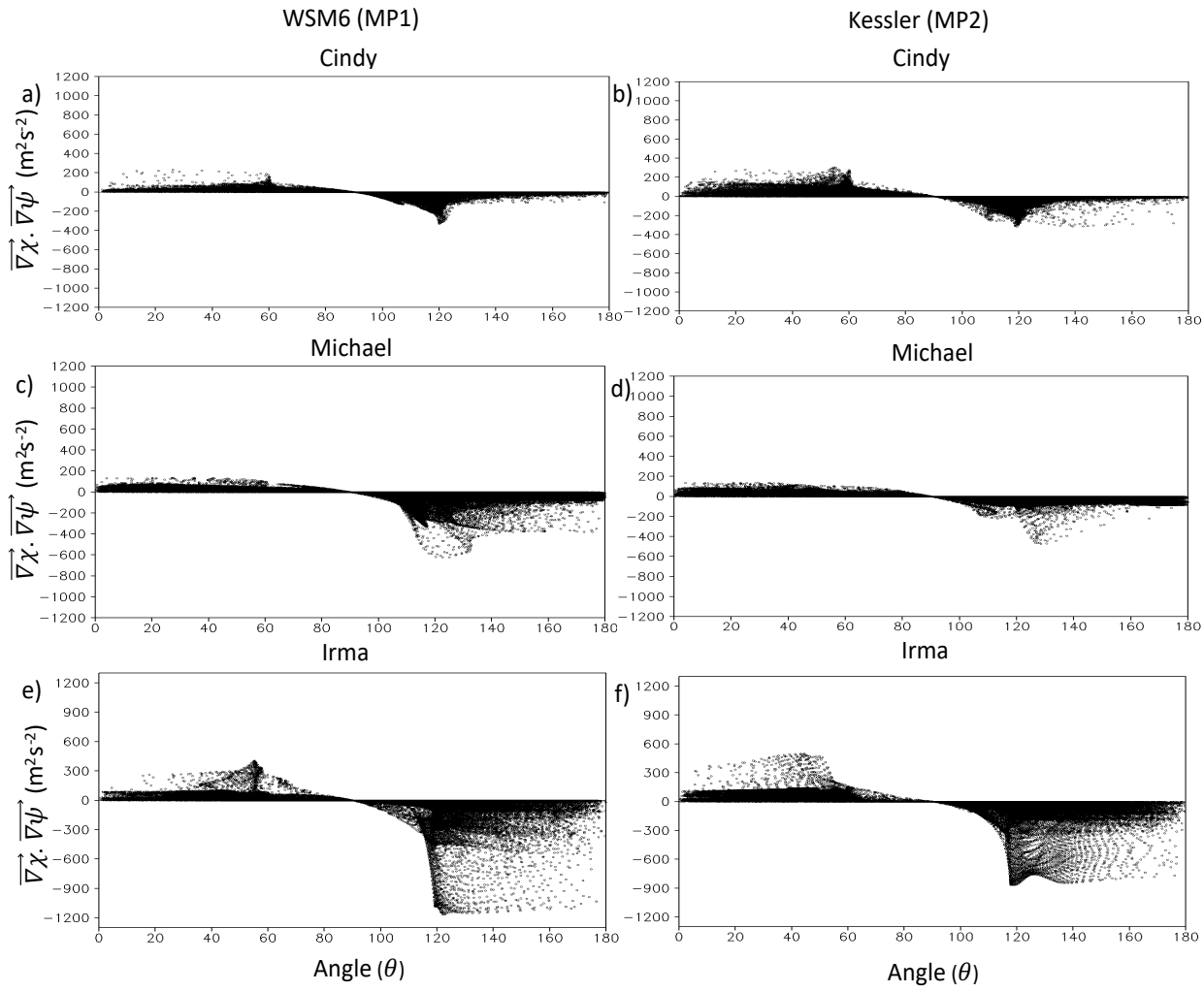

Figure 22. $(\nabla\psi.\nabla\chi)$ as a function of the angle (in degrees) between the gradients of ψ and χ at outflow level of TCs (a, b) Cindy 2017, (c, d) Michael 2018 and (e, f) Irma 2017 when they reach their peak intensity. (a, c, e) for WSM6 and (b, d, f) for Kessler.

Table 5: The tally of the points with positive and negative orientation of the gradients of ψ and χ in Figs. 21 and 22.

Figure 21 (at 850hPa)						
TC	Cindy		Michael		Irma	
Microphysics	WSM6	Kessler	WSM6	Kessler	WSM6	Kessler
Angle < 90	28443	26184	32428	29524	37291	34297
Angle > 90	25812	26002	20071	25168	17709	21566
Figure 22 (at outflow level)						
TC	Cindy		Michael		Irma	
Microphysics	WSM6	Kessler	WSM6	Kessler	WSM6	Kessler
Angle < 90	39818	38244	30941	32837	25407	30921
Angle > 90	40244	35527	48827	42356	57775	50147

c) Understanding the sensitivity of the TC simulations to changes in stage of evolution

Next set of figures (Fig.23 – Fig.27) describe how $\psi - \chi$ framework can be used to understand the evolution of tropical cyclone from its initiation marked as developing stage to maturity marked as intensifying stage. For this we picked three TCs (described in Table 1 and 2) both for developing and intensifying stage simulated with WSM6. Here we picked only one microphysics as earlier we have seen the clear distinction between WSM6 (MP1) and Kessler (MP2) for intensifying stage. Figure 22 shows the evolution of the kinetic energies from the genesis to the intensifying stage. At 850hPa, over the time period of the evolution of the TC, the non-divergent kinetic energy increases and the irrotational kinetic energy decreases for both stages across all three TCs. The only difference occurs in terms of their range of values between the intensifying stage ('phase B') relative to the developing stage ('phase A'). This result in Fig. 23 implies that energy available to be transformed from irrotational non-divergent kinetic energy at 850 hPa is higher in phase B than

in phase A. At the intensifying stage the outflow layer lies at 300hPa, 250hPa, and 200hPa for tropical cyclones Cindy, Michael and Irma, respectively. Whereas it is 400hPa, 350hPa and 250hPa at the developing stage (level determined at the time of peak intensity for each storm at each stage) for tropical cyclones Cindy, Michael and Irma, respectively.

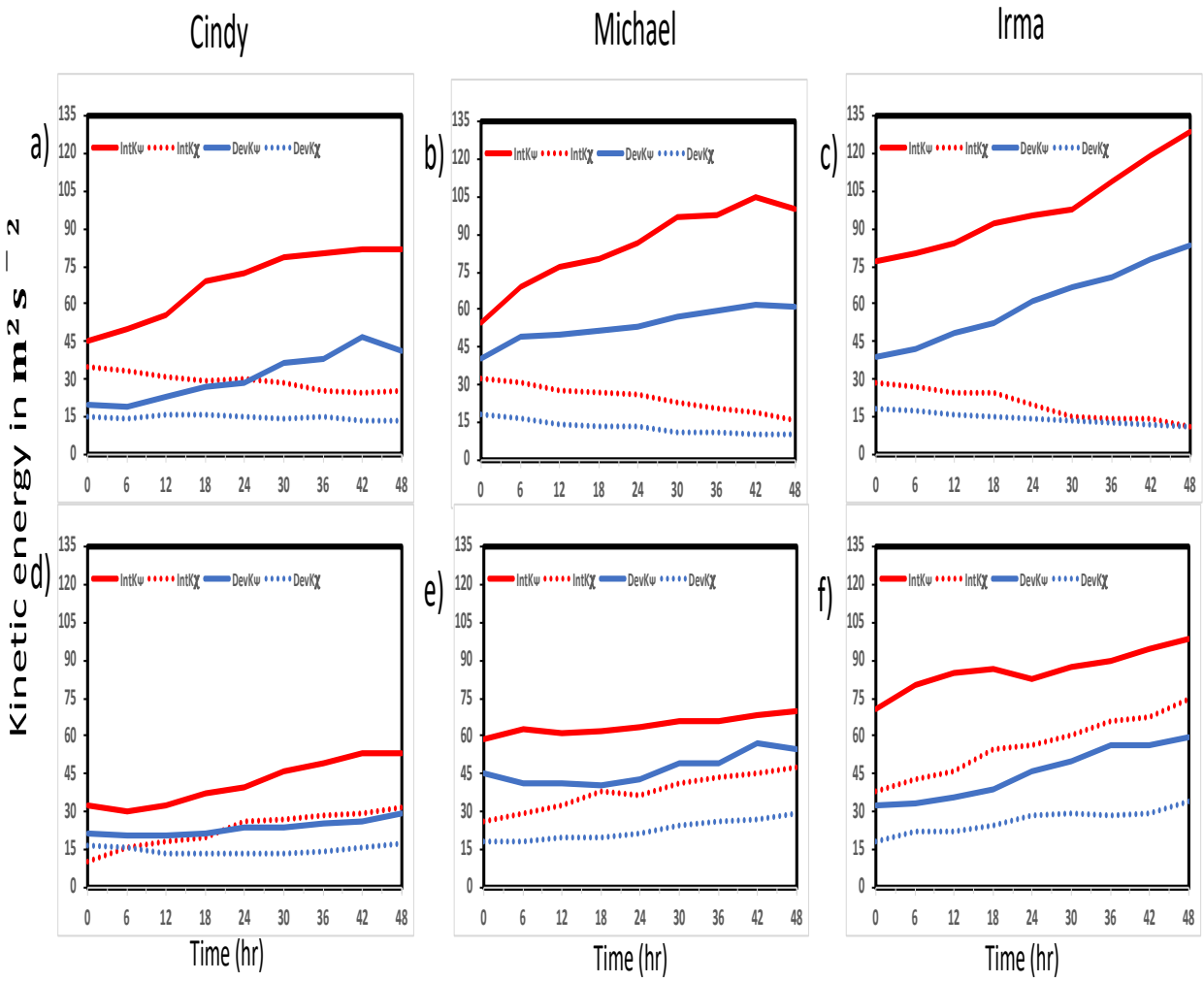

Figure 23. The time series of the irrotational (K_χ) and nondivergent (K_ψ) kinetic energy for (a, d) Cindy 2017, (b, e) Michael 2018, and (c, f) Irma 2017 for (a, b, c) 850hPa and (d, e, f) outflow simulations. The red and blue lines in each panel are for the Intensifying and developing stages.

At 850hPa, generally, available potential energy increases from Cindy to Michael to Irma implying more energy availability for stronger cyclones in both phases. Term 1, Term 2 and Term 3 from Equation 32 shows an increasing trend but the values are one or two orders of magnitude smaller in phase A compared to phase B (Figs. 24 a, b, c) proving a point that intensification of a storm requires rigorous production of non-divergent kinetic energy to support a stronger circulation around low pressure system compared to the incipient state. When individual terms are compared within each phase (Figs. 24 d, e and f), Term 1 is greatest in intensifying stage but Term 2 in developing stage holds highest value throughout the time for all cases. For the developing stage, Term 2 is more important because it is associated with the production of non-divergent energy in the vicinity of the primary circulation.

As the height of outflow level changes from the developing to the intensifying stage it is expected that the time evolution of the individual terms would also change. But the inherent nature of decreasing trend of Term1, Term 2, Term 3 and increasing trend of Term 5 described as APE are present here also. Figure. 25 (a, b and c) depicts changes for intensifying stages and the nature of change already explained in Fig 16. But for the developing stage (Fig. 25 d, e and f) the values of individual terms (Term1, Term 2 and Term3) are no longer negative for Cindy and Michael though for Irma they are negative for 36^{th} hour - 48^{th} hour of the simulation but remained positive for rest of the period.

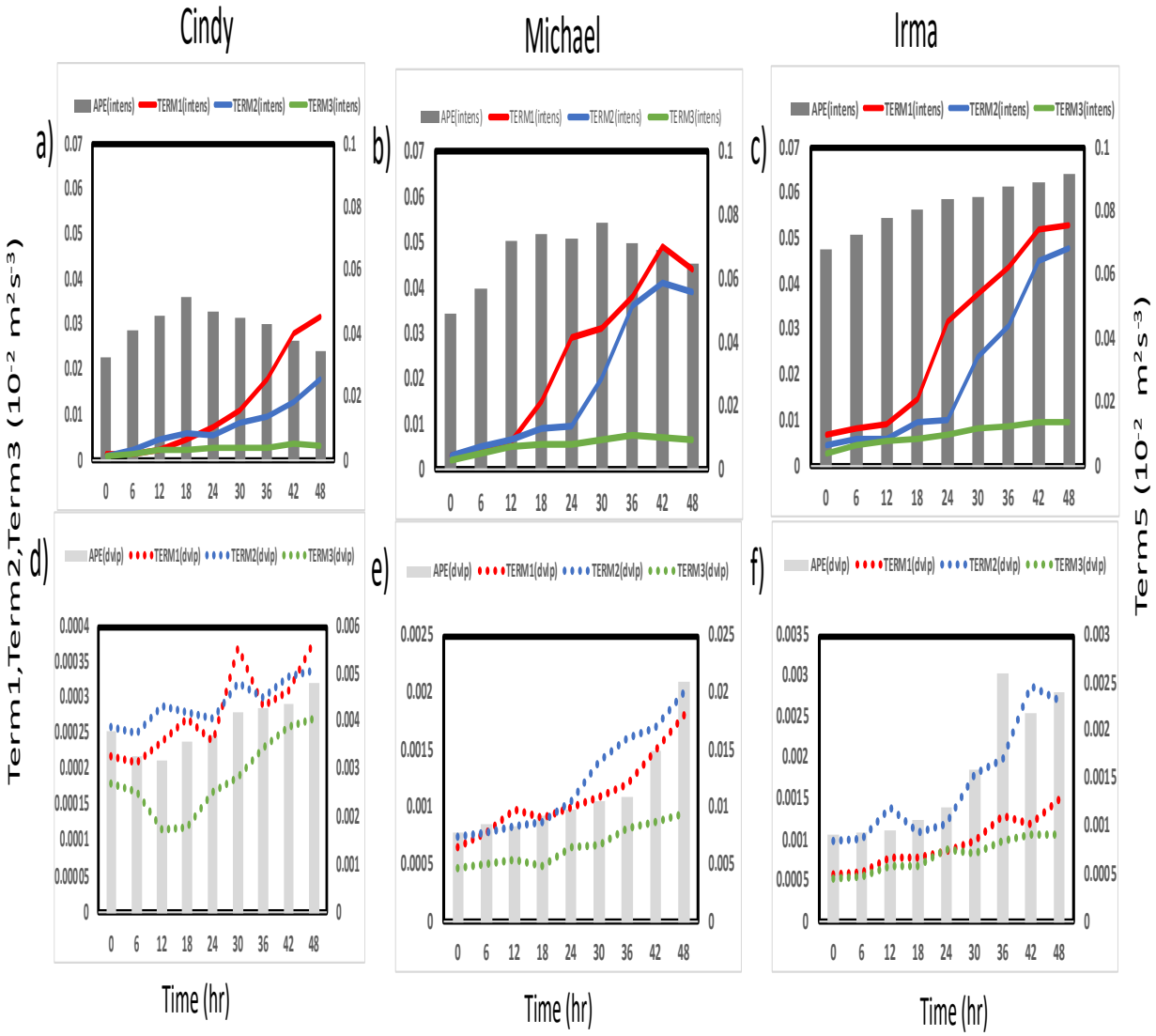

Figure 24. The transformation terms (see Equation 32) at 850 hPa for TC (a, d) Cindy 2017, (b, e) Micheal 2018, and (c, f) Irma 2017. (a, b,c) for intensifying stage and (d, e, f) for developing stage. The dotted and solid lines in each panel are for the developing and intensifying stages of the TC.

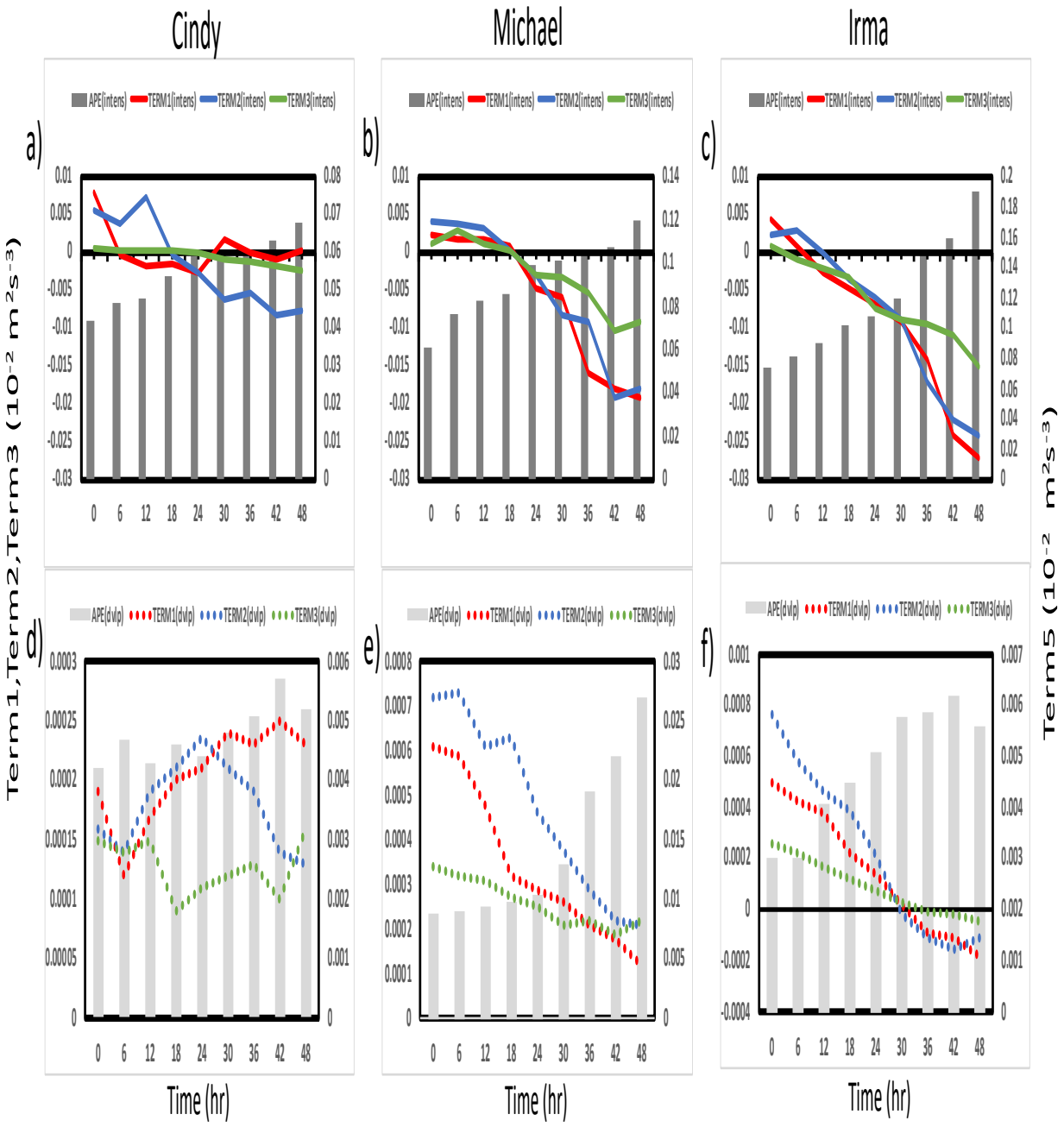

Figure 25. The transformation terms (see Equation 32) at outflow level for TC (a, d) Cindy 2017, (b, e) Micheal 2018, and (c, f) Irma 2017. (a, b, c) for intensifying stage and (d, e, f) for developing stage. The dotted and solid lines in each panel are for the developing and intensifying stages of the TC.

All of these energy exchanges are facilitated by the orientation of the gradient of psi and chi field. More parallel orientation leads to higher amount of non-divergent energy production and antiparallel orientation hinder the transformation. As described before (Fig. 17, 18 and Table 4) with example of three storms (with WSM6) showed importance of orientation and how they changed with changing levels. More specifically saying for intensification of TCs, lower level i.e. 850hPa require more gradients to be arranged between angles 0^0-90^0 whereas outflow level require them to be aligned in a antiparallel fashion i.e. lie between angles 90^0-180^0. The same thing is observed in Fig. 26 a, c and e for intensification of Cindy, Michael and Irma respectively. But for the development stage the condition will be different as the vortex is less compact it would involve a higher region under consideration for domain average at 850hPa . Larger region (greater number of points from Table 6, 850hPa section) under consideration with low values of dot product (Fig. 26 b, d and f) during developing stage compared to intensifying stage (Fig. 26 a, c and e).

From previous two instances (intensifying TCs and their variation with microphysics), it can be said outflow level is basically a region where the negative value of the dot product of gradients should be dominant for the intensification (here also Fig. 27 a, c, e and Table 6) of any scenario (here all three TCs). But the question is whether the same thing is true for developing cases. If we look Table.6, specifically the number of points under the category of outflow level for developing stage then we find more points under 90^0-180^0 range influencing the diffluence of TCs like the intensifying stage. From the plots of developing stage (Fig 27 b, d and f) it is also evident that like the individual terms, the dot product is smaller in magnitude and levels considered for outflow are different from the intensifying stage (Fig. 27 a, c and e) for all TCs.

But there are distinct differences between the behavior of outflow levels during developing and intensifying stages of every TC. The differences are in terms of height i.e pressure level of the

outflow region as well distribution of grid points with positive/negative values of gradients. In case of all the TCs, points under 0^0-90^0 is higher and points under 90^0-180^0 is lower for developing stage from Fig. 27 b, d, f and Table 6. section - outflow level), when compared to intensifying stage (from Fig. 27 a, c, e and Table 6. section - outflow level), highlighting that the importance of diffluence level is greater during intensifying stage than developing scenario.

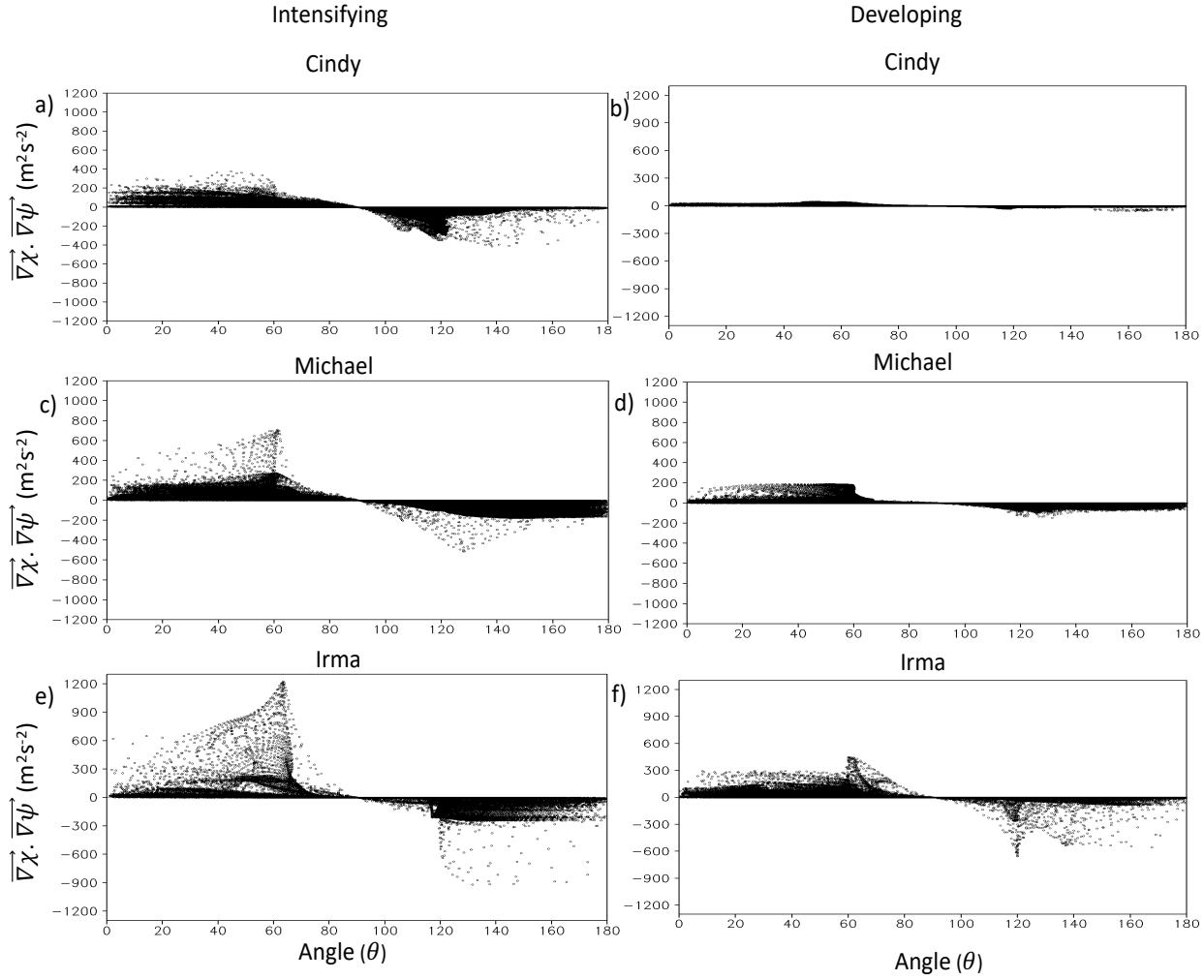

Figure 26. $(\nabla\psi.\nabla\chi)$ as a function of the angle (in degrees) between the gradients of ψ and χ at 850hPa of TCs (a,b) Cindy 2017, (c,d) Michael 2018 and (e,f) Irma 2017 when they reach their peak intensity. (a,c,e) for Intensifying stage and (b,d,f) for Developing stage.

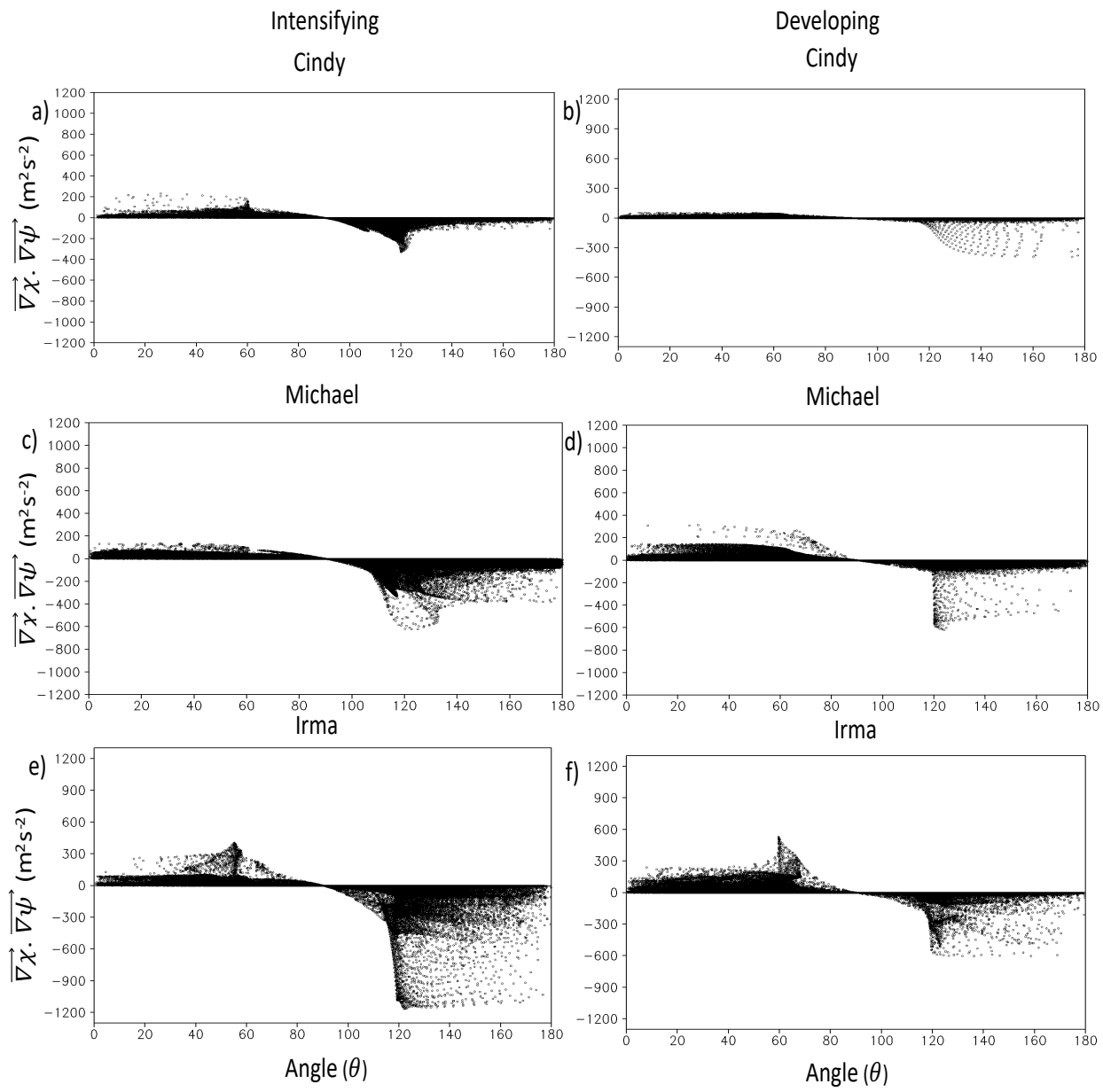

Figure 27. $(\nabla\psi.\nabla\chi)$ as a function of the angle (in degrees) between the gradients of ψ and χ at outflow level of TCs (a, b) Cindy 2017, (c, d) Michael 2018 and (e, f) Irma 2017 when they reach their peak intensity. (a, c, e) for Intensifying stage and (b, d, f) for Developing stage.

Table 6: The tally of the points with positive and negative orientation of the gradients of ψ and χ in Figs. 26 and 27.

Figure 26 (at 850hPa)						
TC	Cindy		Michael		Irma	
Microphysics	Intensifying	Developing	Intensifying	Developing	Intensifying	Developing
Angle < 90	28443	27661	32428	33489	37291	38439
Angle > 90	25812	26236	20071	26326	17709	20028
Figure 27 (at outflow level)						
TC	Cindy		Michael		Irma	
Microphysics	Intensifying	Developing	Intensifying	Developing	Intensifying	Developing
Angle < 90	39818	34743	30941	35965	25407	31564
Angle > 90	40244	34107	48827	36743	57775	40628

CHAPTER 5

CONCLUSION AND FUTURE WORK

In this study we have introduced a framework to understand the evolution of a TC based on the energy transformation between the irrotational and the non-divergent component of the wind. This framework is elegant in that it provides an understanding of the evolution of the TC based on the energy transformation that is physically interpretable based on the relative contributions of its forcing terms. Our analysis reveals that when the gradients of the streamfunction and velocity potential are large and oriented parallel to each other both in the large-scale TC environment and in the region of the primary circulation of the TC, then the TC is favored to intensify with robust conversion of K_χ to K_ψ at 850hPa. In contrast, however in the outflow layer, we require a slower conversion of K_χ to K_ψ for a TC to intensify otherwise it leads to increased inertial instability and weakening of the TC. This conclusion was repeatedly obtained when the contrast of the TC simulations were made across TCs of different intensity, within the lifetime of a TC simulation as it grew from an incipient to a mature stage, and in model simulations where the change in microphysics led to a change in the intensity of the TC from the control simulation.

In this study we conducted several WRF simulations of three different TCs with varied intensity and showed that the $\psi - \chi$ framework is a viable avenue to understand the evolution of these TCs. Of course, for the transformation of K_ψ from K_χ, APE is required, which is dictated by the covariance between the vertical motion and temperature that in turn is dictated by the condensational heating.

In the first scenario, where we compared the simulations of the TCs Cindy, Irma and Michael, we showed that at 850hPa the transformation of APE to K_χ and then to K_ψ was strongest

in the case of Irma followed by that in Michael and then in Cindy. This also reflected the relative intensity of the three TCs with Irma being the strongest followed by Michael and Cindy. This energy transformation manifested similarly with the terms of $\underbrace{\overline{\overline{f\nabla\psi.\nabla\chi}}}_{Term\ 1}, \underbrace{\overline{\overline{\nabla^2\psi\nabla\psi.\nabla\chi}}}_{Term\ 2}, and\ \underbrace{\overline{\overline{\nabla^2\chi\left(\frac{\nabla\psi}{2}\right)^2}}}_{Term\ 3}$ being most dominant in Irma, then in Michael finally followed by Cindy.

In the second scenario, we compared the simulations of each of these TC's in their incipient and mature stages of the simulations. Both these stages of the simulations were diagnosed over a corresponding 48 hour period of simulations. In each of these cases, the relative magnitudes of the energy transformation terms (Term 1, Term 2, and Term 3) at 850hPa unambiguously discriminated the incipient from the mature stage of the TCs. For example, each of these terms were much weaker in magnitude during the incipient stage of the TC compared to the mature stage of the TC.

In the third scenario, we compared the simulations of each of these TCs with two different microphysics schemes: Kessler (which included only the warm rain physics) and WSM6 (which included mixed phase clouds). Except for the case of the incipient stage of the simulation of TC Cindy in all other instances WSM6 simulated a stronger TC than Kessler microphysics. In all of these cases the psi-chi diagnostics at 850hPa very clearly discriminated the relative differences in the intensity simulation of the TC between WSM6 and Kessler schemes with the more intense simulation showing a stronger transformation of kinetic energy from the irrotational to the non-divergent kinetic energy.

Similarly, at the outflow level of the TC, the psi-chi diagnostics is equally revealing. We consistently find that the transformation of $K_\chi\ to\ K_\psi$ is weaker in cases of stronger TC compared

to weaker TC. Again, the three terms (Terms 1, 2, and 3) in the time tendency equations of $K_\chi \; and \; K_\psi$ clearly show the relative differences in the transformation of the energy from $K_\chi \; to \; K_\psi$ at the outflow level. This reduction in K_ψ at the outflow level relates to a corresponding decrease in the inertial stability, which helps in minimizing the resistance to the outflow and therefore further intensification of the TC. Therefore, the relative reduction of the growth in K_ψ in the outflow layer at the expense of K_χ leads to a favorable environment for the intensification of the TC.

Our psi-chi diagnostics also revealed that releasing more APE need not necessarily produce more $K_\chi \; or \; K_\psi$. This is most apparent in the differences in the diagnostics between 850hPa and the outflow level. Even though at the outflow level there is far more condensational heating that is released, the transformation from $K_\chi \; to \; K_\psi$ is weaker. This is because the orientation of the gradients of stream function and velocity potential is not conducive for transformation from $K_\chi \; to \; K_\psi$. Similarly, we find that at the outflow level there is more condensational heat released in the WSM6 microphysics scheme than the Kessler scheme in the incipient stage of TC Cindy. And yet the transformation of $K_\chi \; to \; K_\psi$ was comparable between the two schemes because the orientation of the gradients of stream function and velocity potential was not very favorable for the transformation from $K_\chi \; to \; K_\psi$ in WSM6. It is futile to separate whether the condensational heating causes the kinematic fields to orient in a favorable manner or if the kinematic fields dictate the condensational heating as they are co-evolving. Furthermore, since this framework is set up for domain averaged quantities (which would otherwise make the boundary flux terms in the equations of the time tendency of K_ψ and K_χ to be dominant at the expense of the other forcing terms) it is not possible to isolate the impact of the spatial distribution of the condensational heating on the kinematic field through this framework. Nonetheless, through these extensive set of

examples (12 cases) we have shown that this psi-chi diagnostics framework is a viable method to understand the evolution of a TC.

One of the most critical aspects of the psi-chi diagnostics is the choice of the domain. Our earlier attempts to compute these diagnostics failed with poor choices of the domain that caused the boundary flux terms to overwhelm all other terms in the time tendency equations of K_ψ and K_χ. Very prudent and objective criterion was developed to choose the domain for averaging of the terms so that by definition the boundary flux terms don't overwhelm the equations. In regard to the choice of the domain at 850hPa we choose to find the radius at which the tangential winds no longer decrease but vary asymptotically with the radius. We fix this radius as the lateral boundary at 850hPa. Then we examine the cross-section of the radial winds and find the pressure level of maximum radial winds to fix the outflow level. Then we plot the radial profile of the radial winds and fix the radius where the radial winds vary asymptotically with the radius to fix the lateral boundaries at the outflow level. Since the domain can vary by case and time, these energy transformation terms also reflect in some ways the size of the TC. Furthermore, we also show the fractional conversion of $K_\chi \; to \; K_\psi$ ($\equiv C_{\chi\to\psi} = \left(\frac{K_\psi - K_\chi}{K_\psi}\right) \times 100$) that avoids the dependency to the size of the domain.

Future work

There are many ways that this work could be further extended and explored. We could begin examining the developing and non-developing TCs from easterly waves using these diagnostics. We could explore if there is a predisposition of certain large-scale climate variations to dictate the geometry of the flow in such a way that it has a bearing on the psi-chi interactions of a developing TC.

The role of initial conditions or the sensitivity of the initial conditions on the simulation or the prediction of a TC could be examined using this framework. For example, Krishnamurti et al. (1982) in the context of the Indian summer monsoon simulation carried out experiments to test the sensitivity of the monsoon simulation to initial conditions using this psi-chi framework. With a high resolution multilevel primitive equation model, Krishnamurti et al. (1982) targeted the Indian monsoon simulation for the week of 5th -11th June, 1979 to test its sensitivity to the orientation of $\nabla\Psi$ and $\nabla\boldsymbol{\chi}$. They replaced the irrotational wind components in the control run, at all levels of the model separately by those from late spring, pre onset and post onset periods. The first two experiments showed no evolution of the monsoon at all. But the third experiment that is post onset initial condition generated a vigorous monsoonal activity characterized by strong cross equatorial flow. All three experiments also exhibited different of psi-chi interactions with the maximum generation of the kinetic energy of the non-divergent flow for the post onset case. So with these experiments it is clear that with modest change to the orientation of $\nabla\Psi$ and $\nabla\boldsymbol{\chi}$ in the initial conditions can produce totally different evolution of the monsoon in a short period of the model integration.

To further understand the potential effect of initial condition on evolution of $\psi-\chi$ interaction in a TC, a simple experiment was designed. For this experiment intensification period (8^{th} Oct 1800 UTC – 10^{th} Oct 1800 UTC) of tropical cyclone Michael (2018) was selected. The initial conditions are created using the WRF simulation with Kessler scheme, that simulated a weaker TC than WSM6. This initial condition was used for a 48 hr (intensification phase) WRF simulation with WSM6 microphysics option. Other parameterization scheme remained the same as before. The following flow chart below describes the whole procedure.

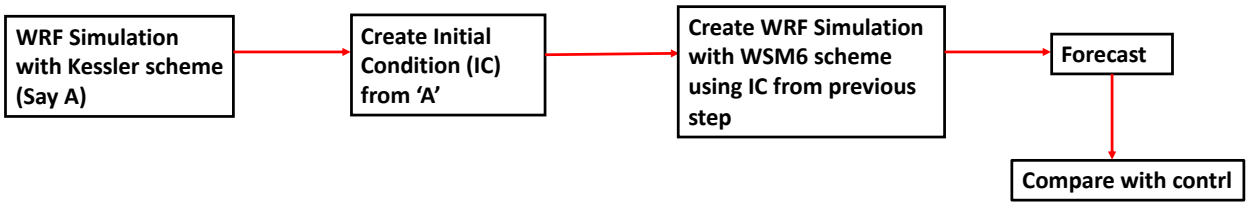

This study will demonstrate the impact of initial conditions on dynamical structure of the tropical cyclone as diagnosed from the psi-chi interactions. As initial conditions created from Kessler scheme simulation would be different from the GFS IC used before (for the control run), it is anticipated that the psi-chi interaction terms computed from the new WSM6 simulation (B run) would vary from the control WSM6 run if the simulations diverge. It was found that the B run simulated a weaker TC Michael than the control run. In fact, this B run simulation was found to be much closer to the control Kessler run (i.e., the B run completed with Kessler scheme instead of the WSM6). We find yet again find that Terms 1, 2, and 3 of the time tendency equations of K_χ *and* K_ψ is able to distinguish the diverging solutions and relate them to the differences in the geometry of the flow, especially the orientation of the stream function and velocity potential. Therefore, from this preliminary experiment we believe that the initial conditions of the kinematic field has a bearing on the evolution of the TC and needs further exploration.

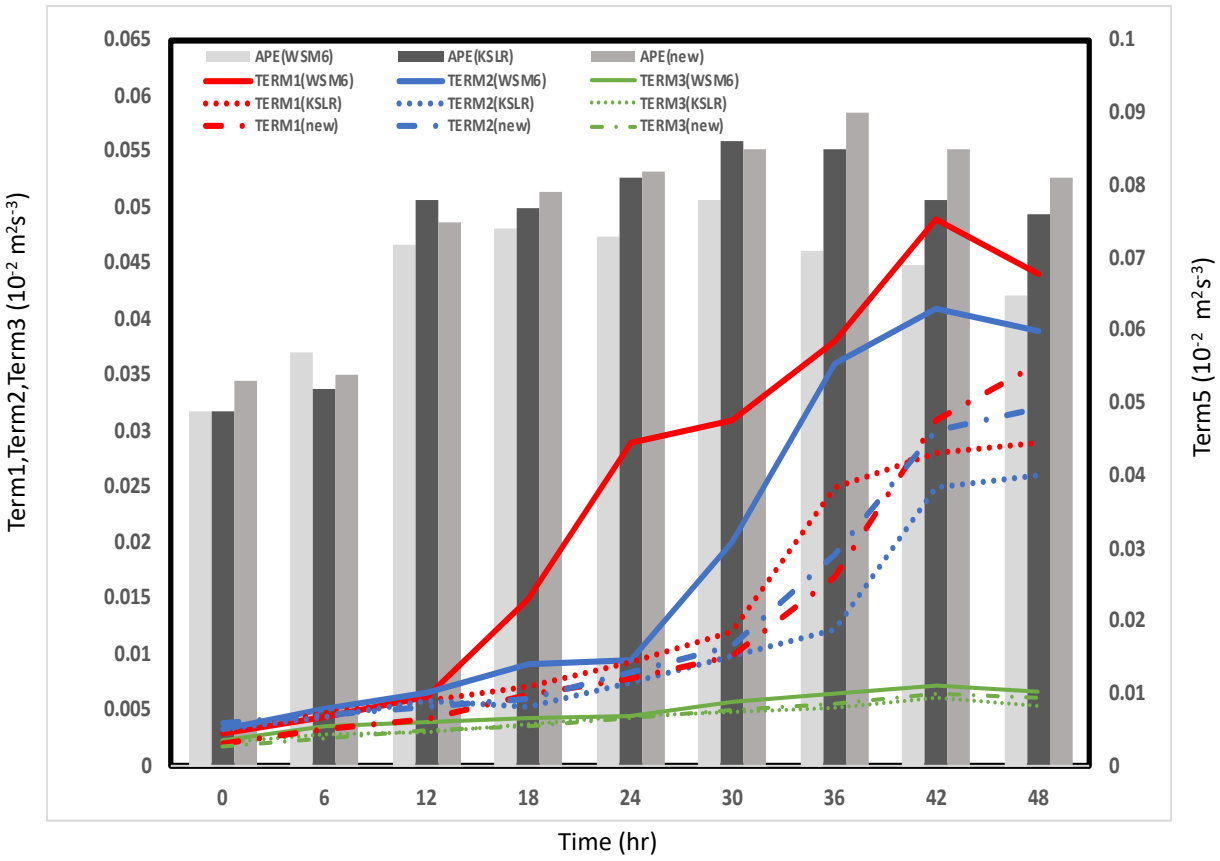

Figure 28. The transformation terms (Terms 1, 2, 3 of Equation 30 and Term 5 of Equation 32) at 850 hPa for TC Michael 2018. Solid lines are for WSM6, dotted lines are for Kessler scheme and dashed lines are for newly initialized model with WSM6.

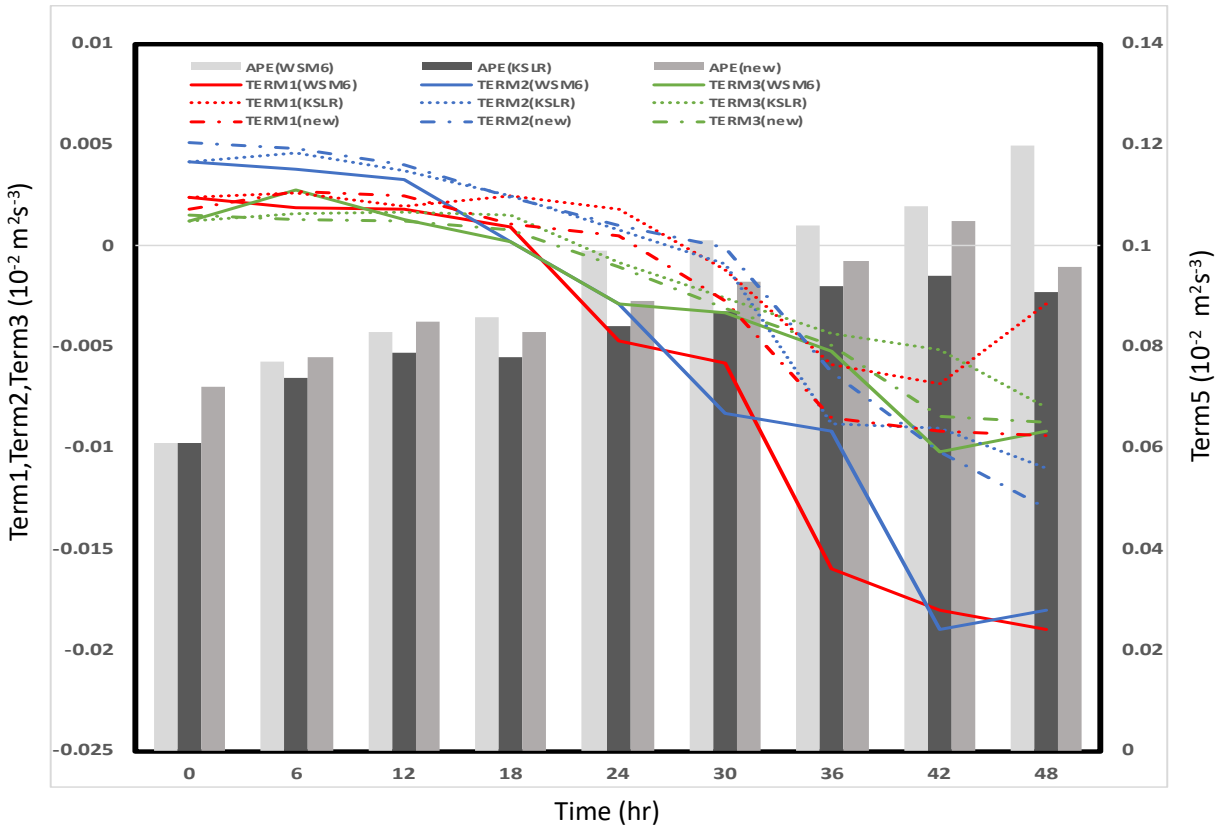

Figure 29. The transformation terms (Terms 1, 2, 3 of Equation 30 and Term 5 of Equation 32) at outflow level for TC Michael 2018. Solid lines are for WSM6, dotted lines are for Kessler scheme and dashed lines are for newly initialized model with WSM6.

REFERENCES

1. Aberson, S. D. (2002), Two years of operational hurricane synoptic surveillance, Weather and forecasting, 17(5), 1101-1110.
2. Aberson, S. D., and J. L. Franklin (1999), Impact on hurricane track and intensity forecasts of GPS dropwindsonde observations from the first-season flights of the NOAA Gulfstream-IV jet aircraft, Bulletin of the American Meteorological Society, 80(3), 421-428.
3. Baker, W. E., R. Atlas, C. Cardinali, A. Clement, G. D. Emmitt, B. M. Gentry, R. M. Hardesty, E. Källén, M. J. Kavaya, and R. Langland (2014), Lidar-measured wind profiles: The missing link in the global observing system, Bulletin of the American Meteorological Society, 95(4), 543-564.
4. Brennan, M. J., D. T. Kleist, K. Howard, and S. J. Majumdar (2015), The impact of supplemental dropwindsonde data on the structure and intensity of Tropical Storm Karen (2013) in the NCEP Global Forecast System, Weather and Forecasting, 30(3), 683-691.
5. Burpee, R. W., J. L. Franklin, S. J. Lord, R. E. Tuleya, and S. D. Aberson (1996), The impact of Omega dropwindsondes on operational hurricane track forecast models, Bulletin of the American Meteorological Society, 77(5), 925-934.
6. Chan, K. T. F., and J. C. L. Chan, 2016: Sensitivity of the simulation of tropical cyclone size to microphysics schemes. Adv. Atmos. Sci., **33**, 1024–1035.
7. Charney, J. G., and A. Eliassen (1964), On the growth of the hurricane depression, Journal of the Atmospheric Sciences, 21(1), 68-75.
8. Chen, S.-H. (2007), The impact of assimilating SSM/I and QuikSCAT satellite winds on Hurricane Isidore simulations, Monthly Weather Review, 135(2), 549-566.
9. Davis, C., W. Wang, S. S. Chen, Y. Chen, K. Corbosiero, M. DeMaria, J. Dudhia, G. Holland, J. Klemp, and J. Michalakes (2008), Prediction of landfalling hurricanes with the advanced hurricane WRF model, Monthly weather review, 136(6), 1990-2005.
10. Emanuel, K. A., J. D. Neelin, and C. S. Bretherton (1994), On large-scale circulations in convecting atmospheres, Quarterly Journal of the Royal Meteorological Society, 120(519), 1111-1143.
11. Franklin, J. L., and M. DeMaria (1992), The impact of Omega dropwindsonde observations on barotropic hurricane track forecasts, Monthly weather review, 120(3), 381-391.
12. Franklin, J. L., S. J. Lord, S. E. Feuer, and F. D. Marks Jr (1993), The kinematic structure of Hurricane Gloria (1985) determined from nested analyses of dropwindsonde and Doppler radar data, Monthly Weather Review, 121(9), 2433-2451.
13. Gray, W. M., and L. Brody (1967), Global view of the origin of tropical disturbances and storms, Citeseer.
14. Hendricks, E. A., M. T. Montgomery, and C. A. Davis (2004), The role of "vortical" hot towers in the formation of tropical cyclone Diana (1984), Journal of the atmospheric sciences, 61(11), 1209-1232.
15. Hong, S.-Y., and J.-O. J. Lim (2006), The WRF single-moment 6-class microphysics scheme (WSM6), J. Korean Meteor. Soc, 42(2), 129-151.
16. Hou, A. Y., S. Q. Zhang, and O. Reale (2004), Variational continuous assimilation of TMI and SSM/I rain rates: Impact on GEOS-3 hurricane analyses and forecasts, Monthly weather review, 132(8), 2094-2109.

17. Houze Jr, R. A., S. S. Chen, W.-C. Lee, R. F. Rogers, J. A. Moore, G. J. Stossmeister, M. M. Bell, J. Cetrone, W. Zhao, and S. R. Brodzik (2006), The hurricane rainband and intensity change experiment: Observations and modeling of Hurricanes Katrina, Ophelia, and Rita, Bulletin of the American Meteorological Society, 87(11), 1503-1522.
18. Iacono, M. J., J. S. Delamere, E. J. Mlawer, M. W. Shephard, S. A. Clough, and W. D. Collins (2008), Radiative forcing by long-lived greenhouse gases: Calculations with the AER radiative transfer models, Journal of Geophysical Research: Atmospheres, 113(D13).
19. Jung, B.-J., H. Kim, F. Zhang, and C.-C. Wu (2012), Effect of targeted dropsonde observations and best track data on the track forecasts of Typhoon Sinlaku (2008) using an ensemble Kalman filter, Tellus A: Dynamic Meteorology and Oceanography, 64(1), 14984.
20. Kain, J. S. (2004), The Kain–Fritsch convective parameterization: an update, Journal of applied meteorology, 43(1), 170-181.
21. Kain, J. S., and J. M. Fritsch (1990), A one-dimensional entraining/detraining plume model and its application in convective parameterization, Journal of the Atmospheric Sciences, 47(23), 2784-2802.
22. Kakar, R., M. Goodman, R. Hood, and A. Guillory (2006), Overview of the convection and moisture experiment (CAMEX), Journal of the atmospheric sciences, 63(1), 5-18.
23. Kavaya, M. J., J. Y. Beyon, G. J. Koch, M. Petros, P. J. Petzar, U. N. Singh, B. C. Trieu, and J. Yu (2014), The Doppler aerosol wind (DAWN) airborne, wind-profiling coherent-detection Lidar system: overview and preliminary flight results, Journal of Atmospheric and Oceanic Technology, 31(4), 826-842.
24. Krishnamurti, T., and Y. Ramanathan (1982), Sensitivity of the monsoon onset to differential heating, Journal of the Atmospheric Sciences, 39(6), 1290-1306.
25. Krishnamurti, T.N., M.C. Sinha, B. Jha, and U.C. Mohanty, 1998: A Study of South Asian Monsoon Energetics. J. Atmos. Sci., **55**, 2530–2548.

26. Krishnamurti, T. N., L. Stefanova, and V. Misra, (2007), Tropical meteorology, Springer.
27. Langford, J. S., and K. A. Emanuel (1993), An unmanned aircraft for dropwindsonde deployment and hurricane reconnaissance, Bulletin of the American Meteorological Society, 74(3), 367-376.
28. Langland, R. H., C. Velden, P. M. Pauley, and H. Berger (2009a), Impact of satellite-derived rapid-scan wind observations on numerical model forecasts of Hurricane Katrina, Monthly Weather Review, 137(5), 1615-1622.
29. Langland, R. H., C. Velden, P. M. Pauley, and H. Berger (2009b), Impact of satellite-derived rapid-scan wind observations on numerical model forecasts of Hurricane Katrina, Monthly Weather Review, 137(5), 1615-1622.
30. Lee, C.-Y., and S. S. Chen (2012), Symmetric and asymmetric structures of hurricane boundary layer in coupled atmosphere–wave–ocean models and observations, Journal of the Atmospheric Sciences, 69(12), 3576-3594.
31. Leslie, L., J. LeMarshall, R. Morison, C. Spinoso, R. Purser, N. Pescod, and R. Seecamp (1998), Improved hurricane track forecasting from the continuous assimilation of high quality satellite wind data, Monthly weather review, 126(5), 1248-1258.
32. Martin, A. C., T. Krishnamurti, and W. K. Lau (2013), Absorbing aerosol-induced change in the early monsoon Arabian Sea low-level jet: Modeled transfer from anomalous heating

to nondivergent kinetic energy, Journal of Geophysical Research: Atmospheres, 118(22), 12,566-512,576.
33. McBride, J. L., and R. Zehr (1981), Observational analysis of tropical cyclone formation. Part II: Comparison of non-developing versus developing systems, Journal of the Atmospheric Sciences, 38(6), 1132-1151.
34. Montgomery, M., M. Nicholls, T. Cram, and A. Saunders (2006), A vortical hot tower route to tropical cyclogenesis, Journal of the atmospheric sciences, 63(1), 355-386.
35. Montgomery, M. T., J. A. Zhang, and R. K. Smith (2014), An analysis of the observed low-level structure of rapidly intensifying and mature hurricane Earl (2010), Quarterly Journal of the Royal Meteorological Society, 140(684), 2132-2146.
36. Montgomery, M. T., J. Persing, and R. K. Smith (2015), Putting to rest WISHE-ful misconceptions for tropical cyclone intensification, Journal of Advances in Modeling Earth Systems, 7(1), 92-109.
37. Montgomery, M. T., N. V. Sang, R. K. Smith, and J. Persing (2009), Do tropical cyclones intensify by WISHE?, Quarterly Journal of the Royal Meteorological Society: A journal of the atmospheric sciences, applied meteorology and physical oceanography, 135(644), 1697-1714.
38. Noh, Y., W. Cheon, S. Hong, and S. Raasch (2003), Improvement of the K-profile model for the planetary boundary layer based on large eddy simulation data, Boundary-layer meteorology, 107(2), 401-427.
39. Nolan, D. S., J. A. Zhang, and D. P. Stern (2009a), Evaluation of planetary boundary layer parameterizations in tropical cyclones by comparison of in situ observations and high-resolution simulations of Hurricane Isabel (2003). Part I: Initialization, maximum winds, and the outer-core boundary layer, Monthly weather review, 137(11), 3651-3674.
40. Nolan, D. S., J. A. Zhang, and D. P. Stern (2009b), Evaluation of planetary boundary layer parameterizations in tropical cyclones by comparison of in situ observations and high-resolution simulations of Hurricane Isabel (2003). Part I: Initialization, maximum winds, and the outer-core boundary layer, Monthly weather review, 137(11), 3651-3674.
41. Nolan, D. S., J. A. Zhang, and D. P. Stern (2009c), Evaluation of planetary boundary layer parameterizations in tropical cyclones by comparison of in situ observations and high-resolution simulations of Hurricane Isabel (2003). Part I: Initialization, maximum winds, and the outer-core boundary layer, Monthly weather review, 137(11), 3651-3674.
42. Penny, A. B., P. A. Harr, and J. D. Doyle (2016), Sensitivity to the representation of microphysical processes in numerical simulations during tropical storm formation, Monthly Weather Review, 144(10), 3611-3630.
43. Reynolds, C. A., P. J. Webster, and E. Kalnay (1994), Random error growth in NMC's global forecasts, Monthly weather review, 122(6), 1281-1305.
44. Riehl, H. (1948), A radiosonde observation in the eye of a hurricane, Quarterly Journal of the Royal Meteorological Society, 74(320), 194-196.
45. Rogers, R., S. Chen, J. Tenerelli, and H. Willoughby (2003a), A numerical study of the impact of vertical shear on the distribution of rainfall in Hurricane Bonnie (1998), Monthly Weather Review, 131(8).
46. Rogers, R., S. Chen, J. Tenerelli, and H. Willoughby (2003b), A numerical study of the impact of vertical shear on the distribution of rainfall in Hurricane Bonnie (1998), Monthly Weather Review, 131(8).

47. Saji NH, G. B., Vinayachandran PN, Yamagata T (1999), A dipole mode in the tropical Indian Ocean. , edited.
48. Shin, S., and R. K. Smith (2008), Tropical-cyclone intensification and predictability in a minimal three-dimensional model, Quarterly Journal of the Royal Meteorological Society, 134(636), 1661-1671.
49. Skamarock, W. C., J. B. Klemp, J. Dudhia, D. O. Gill, D. M. Barker, W. Wang, and J. G. Powers (2005), A description of the advanced research WRF version 2Rep., National Center For Atmospheric Research Boulder Co Mesoscale and Microscale Meteorology Div.
50. Smith, R. K., and M. T. Montgomery (2015), Toward clarity on understanding tropical cyclone intensification, Journal of the Atmospheric Sciences, 72(8), 3020-3031.
51. Smith, R. K., and M. T. Montgomery (2016), The efficiency of diabatic heating and tropical cyclone intensification, Quarterly Journal of the Royal Meteorological Society, 142(698), 2081-2086.
52. Smith, R. K., M. T. Montgomery, and S. Vogl (2008), A critique of Emanuel's hurricane model and potential intensity theory, Quarterly Journal of the Royal Meteorological Society: A journal of the atmospheric sciences, applied meteorology and physical oceanography, 134(632), 551-561.
53. Smith, R. K., M. T. Montgomery, and N. Van Sang (2009), Tropical cyclone spin-up revisited, Quarterly Journal of the Royal Meteorological Society: A journal of the atmospheric sciences, applied meteorology and physical oceanography, 135(642), 1321-1335.
54. Van Sang, N., R. K. Smith, and M. T. Montgomery (2008a), Tropical-cyclone intensification and predictability in three dimensions, Quarterly Journal of the Royal Meteorological Society, 134(632), 563-582.
55. Van Sang, N., R. K. Smith, and M. T. Montgomery (2008b), Tropical-cyclone intensification and predictability in three dimensions, Quarterly Journal of the Royal Meteorological Society, 134(632), 563-582.

BIOGRAPHICAL SKETCH

Sweta Das was born and raised at Kolkata, India. Being near to Bay of Bengal, Kolkata has lot of weather events, such as summer thunderstorm, monsoon rain and then got post monsoon low pressure systems. That always intrigued her. After completing her undergraduate with Physics, Mathematics and Chemistry, she decided to pursue Masters in Atmospheric Science from University of Calcutta. Post Masters she joined India Meteorological Department as senior research fellow and worked there for two years. Here she worked on a project involving effect of weather on agriculture using a statistical model. She joined FSU as a visiting scholar in Late Prof. T. N. Krishnamurti's lab. Here she worked on Indian summer monsoon and published two articles. In 2014 she joined FSU as a graduate student under the supervision of Late Prof. T. N. Krishnamurti. Here she worked on NASA CPEX, 2017 field phase experiment as a student forecaster and flew to tropical cyclone Cindy (2017). Later she continued the same work under the supervision of Dr. Vasubandhu Misra and Dr. Guosheng Liu.